



Assessing engineered tissues and biomaterials using ultrasound imaging: *In vitro* and *in vivo* applications



Joseph A. Sebastian^{a,b,*}, Eric M. Strohm^{b,c}, Jérôme Baranger^d, Olivier Villemain^{d,e}, Michael C. Kolios^{f,g,h}, Craig A. Simmons^{a,b,c,*}

^a Institute of Biomedical Engineering, University of Toronto, Toronto, Canada

^b Translational Biology and Engineering Program, Ted Rogers Center for Heart Research, Toronto, Canada

^c Department of Mechanical and Industrial Engineering, University of Toronto, Toronto, Canada

^d Labatt Family Heart Centre, The Hospital for Sick Children, University of Toronto, Toronto, Canada

^e Department of Medical Biophysics, University of Toronto, Toronto, Canada

^f Department of Physics, Toronto Metropolitan University, Toronto, Canada

^g Institute of Biomedical Engineering, Science and Technology (iBEST), A Partnership Between Toronto Metropolitan University and St. Michael's Hospital, Toronto, Canada

^h Keenan Research Centre for Biomedical Science, Li Ka Shing Knowledge Institute, St. Michael's Hospital, Toronto, Canada

ARTICLE INFO

Keywords:

Non-invasive imaging
Ultrasound imaging
Engineered tissues
Organ-on-a-chip
Ultrafast ultrasound imaging
Elastography

ABSTRACT

Quantitative assessment of the structural, functional, and mechanical properties of engineered tissues and biomaterials is fundamental to their development for regenerative medicine applications. Ultrasound (US) imaging is a non-invasive, non-destructive, and cost-effective technique capable of longitudinal and quantitative monitoring of tissue structure and function across centimeter to sub-micron length scales. Here we present the fundamentals of US to contextualize its application for the assessment of biomaterials and engineered tissues, both *in vivo* and *in vitro*. We review key studies that demonstrate the versatility and broad capabilities of US for clinical and pre-clinical biomaterials research. Finally, we highlight emerging techniques that further extend the applications of US, including for ultrafast imaging of biomaterials and engineered tissues *in vivo* and functional monitoring of stem cells, organoids, and organ-on-a-chip systems *in vitro*.

1. Introduction

Advances in regenerative medicine, tissue engineering, and biomaterials-based therapies towards clinical applications demand non-invasive tools to quantitatively assess functional outcomes *in vivo*. Similarly, *in vitro* applications of regenerative medicine and tissue engineering – including induced pluripotent stem cell-derived (iPSC) disease modeling, organoids, and organ-on-a-chip applications – require quantitative methods to assess structure and function, particularly longitudinally (i.e., monitoring cell and tissue function over time in culture).

Imaging methods broadly meet these requirements by enabling non-invasive and non-destructive visualization of structures, and are frequently used for the assessment of engineered tissues and biomaterials *in vivo* and *in vitro* [1–5]. Beyond structure, some medical imaging modalities also enable quantitative *functional* assessment across

multiple length scales, from organs to organelles. Ultrasound (US) imaging is a cost-effective option in this context, as it can be used not only for its familiar clinical applications of imaging tissue structure and blood flow, but also to quantitatively assess acoustic, mechanical, and other tissue properties. Further, ultrasound spatial resolution can be tuned to specific applications by adjusting the central frequency of the ultrasonic transducer from the centimeter-scale at the low frequencies (<10 MHz) used in clinical US scanners to the micron-scale at high frequencies (>200 MHz) that are needed for *in vitro* assessment of cells and microtissues.

Here we review applications and opportunities for the use of US in regenerative medicine, tissue engineering, and biomaterials research and development. We provide a primer on the theoretical basis of US techniques to assess the properties of cells, tissues, and biomaterials (Section 2); review *in vitro* and *in vivo* applications of US relevant to regenerative medicine (Section 3); and discuss significant future opportunities for US imaging in this field (Section 4).

* Corresponding authors. Institute of Biomedical Engineering, University of Toronto, Toronto, Canada.

E-mail addresses: j.sebastian@mail.utoronto.ca (J.A. Sebastian), c.simmons@utoronto.ca (C.A. Simmons).

List of abbreviations

US	ultrasound
iPSC	induced pluripotent stem cell
TE	tissue engineering
USE	ultrasound elastography
A-mode	amplitude-mode
B-mode	brightness-mode
C-mode	contrast-mode
M-mode	motion-mode
QUS	quantitative ultrasound
BSC	backscatter coefficient
IBC	integrated backscatter coefficient
ARF	acoustic radiation force
AFM	atomic force microscopy
PDMS	polydimethylsiloxane
MSSER	monitored steady-state excitation and recovering
HA	hyaluronic acid
GWE	guided wave elastography
OOAC	organ-on-a-chip
FUS	focused ultrasound

2. Fundamentals of ultrasound imaging for tissue engineering

The following sections describe the fundamentals of US imaging to contextualize the innovation of the applications of US to tissue

engineering (TE) described in Sections 3–5.

2.1. Fundamentals of ultrasound

Ultrasound (US) describes sound at an ultrasonic frequency (i.e., above the audible range or >20 kHz). In biomedical applications, US imaging describes the use of these high-frequency sound waves to penetrate biological tissue to either: 1) generate images of internal organs [6] or maps of organ/tissue function [7]; or 2) interact with tissues or organs to deform, heat, or deliver drugs to specific parts of the body [8]. In this Review, we mainly focus on the former to evaluate *in vitro* and *in vivo* biomaterials and bioengineered tissues. In addition, we describe the use of ultrasound elastography (USE) in these applications, in which US deforms tissue to generate parametric maps from which one can infer organ/tissue function. The experimental requirements of an ultrasonic system for evaluation of engineered tissues and biomaterials (e.g., imaging frequency, imaging mode) depend on factors such as the size of the biological structures of interest (i.e., this determines the spatial resolution of the US system required to visualize these structures) and the ultrasonic properties of the engineered tissue or biomaterial (e.g., acoustic attenuation).

2.1.1. Attenuation

Acoustic attenuation refers to the energy loss of an US beam as it passes through a medium and is composed of absorption and scattering [9]. As the US wave propagates through the medium, the energy can be absorbed or scattered. Energy loss due to attenuation is manifested as a decrease in amplitude of the US beam as a function of distance as it passes through the medium. Attenuation is frequency-dependent

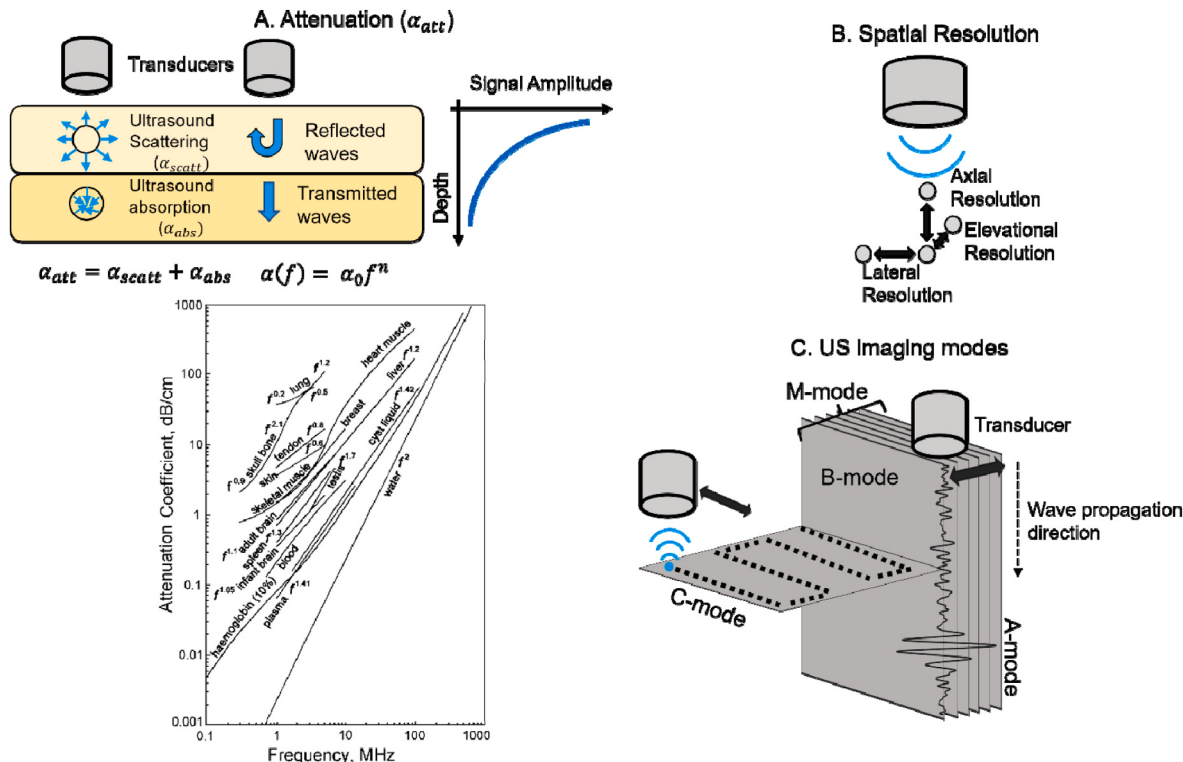


Fig. 1. Fundamental considerations in applications of US to a TE application. (A) Schematic of the main contributions to the ultrasonic attenuation coefficient (α_{att}), composed of the addition of the contributions of ultrasound scattering (α_{scatt}) and ultrasound absorption (α_{abs}) on for a single scatterer (left), and the impact of ultrasound attenuation in a layered system (middle) where ultrasound signal amplitude decreases as a function of sample depth due to wave reflection at interfaces (right) and the ultrasound attenuation coefficient values increase as a function of ultrasonic frequency. Here, $\alpha(f)$ represents the frequency-dependent attenuation function, α_0 represents the attenuation coefficient of the biological tissue, f represents the frequency of the US waves in the tissues, and n lies between 1.0 and 2.0 for soft tissues in biological media. A plot of frequency-dependent attenuation for common biological media is depicted in the bottom left of the figure, taken from Ref. [16]. (B) Schematic depiction of lateral, axial, and elevational resolution. (C) Schematic depiction of the different types of US imaging modes described in Section 2.1.3 modified and adopted from Ref. [3].

(absorption and scattering can also be frequency-dependent) and tissue- and organ-dependent (Fig. 1A). For soft biological tissues, the frequency-dependent attenuation is described by the following power law: $\alpha(f) = a_0 f^n$, where $\alpha(f)$ represents the frequency-dependent attenuation function, a_0 represents the attenuation coefficient of the biological tissue, f represents the frequency of the US waves in the tissues, and n lies between 1.0 and 2.0 for soft tissues (Fig. 1) [9]. Attenuation coefficients of various native biological tissues and the corresponding n values are published [10]; generally, tissues that have high water content have n values closer to 2 while those with low water content are closer to 1. n values for engineered tissues and biomaterials, while not generally published, can be determined using attenuation estimation methods [11–16].

The contribution of absorption and scattering to the total attenuation depends on the frequency of the ultrasound wave. At low-MHz frequencies, scattering is ~10–15% of the total attenuation whereas the absorption accounts for the remaining ~85–90% of the acoustic attenuation [15–18]. As the central frequency of the transducer is increased (in the MHz range), the influence of acoustic scattering typically increases [19]. Thus, for *in vitro* models that use higher frequency US systems (Section 3.2, 3.3, 4.2, 4.3), scattering can contribute more significantly to the overall tissue attenuation.

The scattering from tissues and their constituents (including cells) is frequency-dependent. In soft biological tissues, scattering from tissue constituents is relatively weak and the frequency dependency can be estimated by the Born approximation [20], which allows solutions to scattering from simple objects, like cells within tissues. When the scattering structure is much smaller than the ultrasound wavelength, the amount of scattering can be approximated from the structure using Lord Rayleigh's equation; this phenomena is referred to as Rayleigh scattering [20]. When the product of the wavenumber (spatial frequency of the wave) and the scatterer size approaches 1, the backscattering power increases, with a more complex frequency dependence [19]. In this regime, the shape and size of the scatterer must be considered to understand the impact of acoustic scattering in biological media. In engineered tissues and biomaterials applications, the most common scatterers are biological cells, which have non-uniform shapes and sizes. As described in Section 2.2.1, 2.2.2 and 3.2, researchers have employed quantitative ultrasound techniques (e.g., spectral analysis, backscatter coefficient estimation) to estimate scatterer size, shape, and concentration to account for and understand this phenomenon [19,20].

2.1.2. Resolution

Depending on the application, engineered tissues and biomaterials are generally manufactured on a micrometer to centimeter scale. Assessment tools employed in these applications, such as US imaging systems, must be able to resolve structures and infer tissue function at these scales. US emission frequency has an inversely proportional relationship to US wavelength, where shorter wavelengths resolve finer details and generate high resolution US images.

The spatial resolution of the US images is in three different dimensions: axial resolution, lateral resolution, and elevational resolution (Fig. 1B), each of which depends on the frequency of the US beam. Axial resolution refers to the ability of a system to resolve particles along the direction of propagation of the ultrasound pulse and depends on the pulse length [9]: as the pulse length depends on the frequency, the higher the emission frequency, the higher the axial resolution. Lateral resolution describes the ability to distinguish objects that are located next to each other at the same imaging depth. Generally, lateral resolution is larger than the axial resolution. Lateral resolution depends on the width of the acoustic beam: narrower beams can discern two scatterers better than a wider acoustic beam. The width of the acoustic beam is determined by the ultrasonic focusing, which also depends on the center frequency of the transducer. As the width of the ultrasonic beam is inversely related to frequency, the higher the frequency, the higher the lateral resolution. The elevational resolution is given by the

slice-thickness dimension of the ultrasound beam perpendicular to the image plane. Similar to the lateral resolution, elevational resolution depends on the transducer design, specifically the manufactured dimensions of the transducer element in an ultrasound array, and the center frequency of the transducer. Reduced transducer element dimensions leads to reduced beam height and better elevational resolution. Like lateral resolution, the transducer element height is inversely related to frequency: the higher the frequency, the higher the elevational resolution. Although higher frequency US systems provide high spatial resolution (i.e., axial, lateral, elevational resolution), they have low penetration depth and stronger attenuation effects, which affects the signal-to-noise ratio (SNR) of the US images in all imaging modes. This is a key trade-off in US imaging: higher frequency waves have shorter imaging depths of penetration with fine spatial resolution and lower frequency waves have larger imaging depths of penetration with coarser spatial resolution. For example, tissue scatterers that cannot be resolved in US images due to the coarse spatial resolution of the system due to their small size leads to the appearance of speckle in the images [19]. In general, *human* applications are evaluated with clinical US systems operating at low frequencies between 1 and 10 MHz to penetrate centimeters deep into tissue with adequate spatial resolution. In contrast, *in vitro* applications with millimeter-sized tissues will generally require the higher spatial resolution of high frequency systems (>100 MHz) with the trade-off of more limited micron-level (1–100 μm) penetration depths.

2.1.3. Ultrasound imaging modes

High frequency US systems can resolve micron-sized (1–100 μm) structures. Using common US imaging modes, these structures can be resolved and their anatomical and functional properties analyzed. The four commonly used US imaging modes to evaluate engineered tissues and biomaterials are: Amplitude Mode (A-Mode), Brightness Mode (B-Mode), Constant Range Mode (C-Mode), and Motion-Mode (M-Mode) (Fig. 1C). In A-mode, the height of the amplitude of a single reflected US pulse (called an echo) is detected and plotted as a one-dimensional line of amplitude versus echo time (also called fast time). This plot is also called an A-line, where fast time represents the time of detection for the US echo [21]. The analysis of multiple A-scan signal acquisitions across acquisition time is known as time-domain analysis, and analysis of the corresponding frequency spectrum of these time-domain A-scan signals is referred to as frequency-domain analysis. A-mode provides spatially localized data, but only in one dimension. In B-mode, A-scans at different locations are combined spatially to yield a single 2-D B-mode image [21]. Here, the intensity of a pixel in a B-mode image is defined by the amplitude at each time point in the A-mode scan. C-scan images depict 2-D grayscale images of planes (cross-sections), generated perpendicular to the direction of the US pulse [21]. Lastly, M-mode consists of a rapid sequence of A-mode scans that are taken across time for a time-dependent measurement of organ/tissue movement relative to the transducer [21]. These imaging modes (A-, B-, C-, and M-mode) can be analyzed via quantitative US techniques (described in Section 3.2) to infer information about tissue function and deduce the structural, and mechanical properties of engineered tissues and biomaterials. Although not discussed in this Review, Doppler US imaging is another imaging mode that is used clinically to visualize and analyze blood flow [21]. Briefly, Doppler US imaging measures the movement of acoustic scatterers through the path of the acoustic beam as a phase change in the received signal. This phase change can be used to measure the displacement and/or the velocity of the acoustic scatterers (e.g., during tissue motion or for blood flow velocity assessment).

2.2. Fundamentals of quantitative ultrasound imaging techniques: backscatter coefficient estimation, spectral analysis, and deducing mechanical properties

Quantitative US (QUS) refers to the development of imaging

measurement methods that yield tissue properties that are independent of instrumentation [20]. In QUS, biologically relevant information is extracted from US images (e.g., acquired in A-mode, B-mode, C-mode, or M-mode) in the time- and frequency-domain. Conventional A-mode, B-mode, C-mode, and M-mode US images are constructed from the ultrasound backscattered from different tissue structures that are recorded as time-domain signals. However, frequency information from these time domain signals can quantify biological information (e.g., number, size, concentration, density, and organization of tissue scatterers) about the tissue of interest and forms the basis of the field of QUS imaging. Quantitative ultrasound techniques are described in this section and summarized in Table 1.

2.2.1. Backscatter coefficient estimation

Cells within native and engineered tissues act as scatterers with varying shapes, sizes, organizations, and impedance mismatches between the cells and the surrounding media. The frequency-dependent relationship of US scattering [20] (described in Section 2.1.1) led to the development of QUS methods that can be used to extract microstructural features of a biological tissue using scattered US waves during an imaging sequence. The backscatter coefficient (BSC) quantifies the amount of differential scattering of US waves in a cross section of tissue per unit volume of that tissue relative to the angle of the incident ultrasound beam [22–24]. Using clinical US systems, the estimation of the BSC has been applied in tissue-mimicking phantoms [25], breast tissue [26], lymph nodes [27], myocardial tissue [28], skin [29], and cell-laden hydrogels [30–32]. The BSC is generally overlaid on B-mode and C-mode images to depict scattering components in 2D imaging slices of the tissue or biomaterial parallel (B-mode) and perpendicular (C-mode) to the imaging transducer (Fig. 2). For example, Mercado et al. estimated a QUS parameter called the integrated backscatter coefficient (IBC), that uses the same principles of the BSC but estimates the backscatter strength of sub-resolution scatterers per unit volume over the transducer bandwidth and provides an approximation of the cell density (Fig. 2) [30–32].

2.2.2. Spectral analysis

While conventional US imaging does not utilize the frequency content of acquired time-domain signals, previous studies have shown that the frequency content can be used to characterize tissue microstructural features, such as number, size, and organization of tissue scatterers in both *in vitro* and *in vivo* settings [33,34]. Analysis of the frequency-content of the US signals during propagation of an US wave is referred to as spectral analysis. After transformation of time-domain data to the frequency domain via the Fourier transform, the frequency-spectrum data can be fit to a linear regression (where the x-axis is the frequency-spectrum of the US data, and the y-axis is the intensity magnitude of the US backscatter). Characteristics of the linear fit (e.g., slope, y-intercept) have been used to characterize tissue

microstructure such as number, size, and organization of tissue scatterers and biological processes (such as cellular differentiation [35] and apoptosis [36]). The recent use of spectral analysis at high frequencies enabled the characterization of osteoblastic differentiation in 3D collagen hydrogels [37] and has been shown to identify differences between scaffolds from tumor-bearing and tumor-free mice at early stages of disease [38] (Fig. 3).

2.2.3. Estimating the mechanical properties of soft biological tissues

Using USE, QUS can estimate the tissue stiffness (e.g., shear modulus, Young's modulus) of a tissue of interest and overlay color-coded maps of tissue stiffness on conventional B-mode US images. USE is an umbrella term that encompasses acoustic radiation force imaging [39] and different forms of shear wave imaging (shear wave elasticity imaging [40] and supersonic shear imaging [41]).

Many clinical and pre-clinical studies that formed the foundation of USE assumed linear, elastic, isotropic, and incompressible tissue properties when determining the mechanical properties of tissue phantoms and native tissues in animal models. These measurements demonstrated good agreement with mechanical testing that led to adoption of USE as an estimation technique of a tissue's mechanical properties. However, many biological tissues are not linear, elastic, isotropic, or incompressible and require more complex analytical approaches (described at the end of this section).

Most elastographic measurements require external tissue stimulation that causes tissue displacement [42]. In USE systems, the tissue is deformed using either contact or non-contact methods. The external load can produce an acoustic radiation force (ARF) that uses compression waves to deform the tissue in depth, with the peak deformation occurring at the focus of the US source (Fig. 4). The ARF can be calculated by the following equation [9]:

$$F = \frac{2\alpha I}{c_p} \quad (1)$$

where F (N/m^3) is the volumetric force, α (dB/m) is the acoustic absorption, I (W/m^2) is the temporal average intensity of the acoustic beam, and c_p (m/s) is the sound speed in the tissue of interest.

This ARF generates shear waves that propagate through the tissue perpendicular to the direction of the ARF and at a speed that depends on the tissue's shear modulus, with greater propagation speeds in stiffer tissues (Fig. 4). For a linear and isotropic material, the shear modulus (μ) is related to the material density (ρ) and shear wave speed (c_s) by:

$$\mu = \rho c_s^2 \quad (2)$$

For incompressible materials with Poisson's ratio (ν , the negative ratio of the transverse to axial strain) of 0.5, the Young's modulus (E) is related to the shear modulus by:

$$E = 3\mu \quad (3)$$

Table 1
Overview of quantitative ultrasound imaging techniques.

Technique	Concept	Acoustic properties measured	Biomaterial and biological information acquired	References
Backscatter coefficient estimation	Estimated from an analytical formula based on the ratio of the normalized power spectral density of the echo signal to a reference backscatter signal from a strong reflector (e.g., quartz) and measured via raster scans	Speed of sound, acoustic impedance, acoustic attenuation, backscatter coefficient, integrated backscatter coefficient	Bulk elastic modulus, physical density, cell density	14, 15, 22–32, 35, 36, 38, 55–69
Spectral analysis	Linear regression analysis applied to the Fourier-transformed time-domain data of the US signals	Power spectrum, mid-band fit, spectral slope	Number, size, and organization of tissue scatterers	30–32, 33–38, 55, 70–80
Elastic wave propagation analysis	Tissue deformation induces elastic wave propagation whose speed and phase are related to the mechanical properties of the biological tissue	Group velocity, phase velocity, tissue displacement from the time-shift in A-scan signals and visualized in the B- and M-mode images.	Elastic and viscoelastic properties of soft biological tissues (e.g., Young's modulus, shear modulus, anisotropic ratio, storage modulus, loss modulus, shear viscosity) based on analytical models, shear wave attenuation	39–42, 48, 82–110

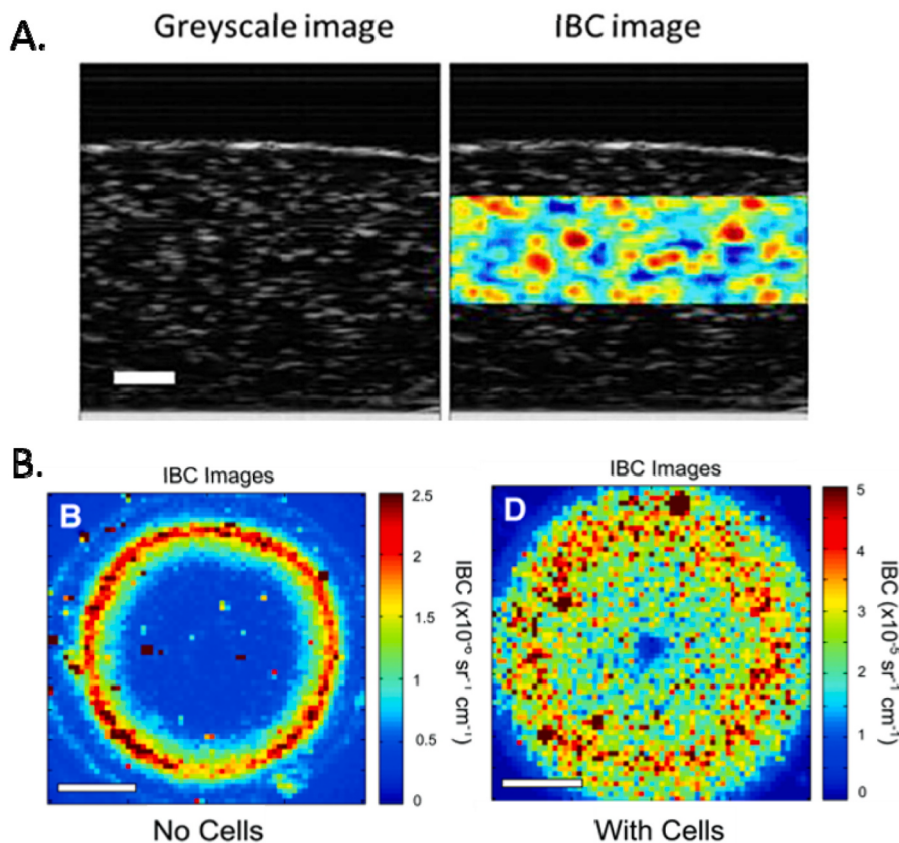


Fig. 2. (A) B-mode grayscale and overlaid integrated backscatter coefficient (IBC) image of PC12 cell-laden hydrogels of 1.0×10^6 cells/ml. The scale bar corresponds to 500 μm – adapted from Ref. [30]. (B) IBC parametric images of acellular (left) and cell-seeded (right) hydrogels – adapted from Ref. [31].

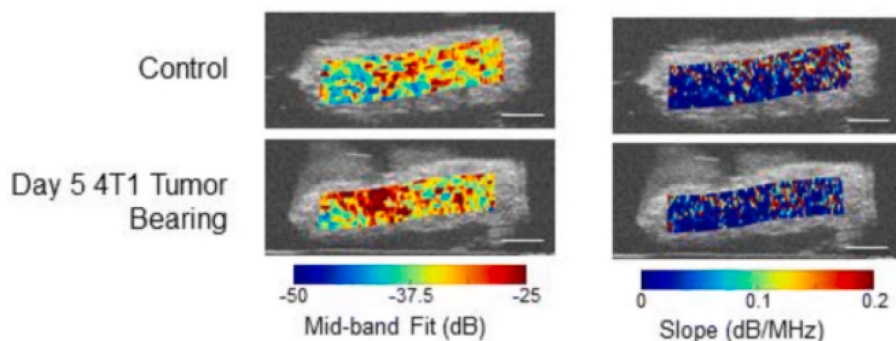


Fig. 3. US spectral analysis employed to differentiate between control (top row) and 4T1 tumor bearing mice at day 5 post-inoculation (bottom row) overlaid with parameter values for the mid-band fit and spectral slope which are main QUS indicators of the cell size, shape, and concentration – adapted from Ref. [38]. The midband fit represents the value of the regression line at the center frequency of the frequency-spectrum of the data (calculated via the Fourier transform of the acquired time-domain data). The spectral slope represents the slope of the line of best fit to the frequency-spectrum data.

Acquisition and frame-to-frame analysis of multiple B-mode images for a specific region of interest across time on the tissue enables reconstruction of a spatiotemporal map of shear wave velocity as a function of lateral position, depth position, and time. From this pixel-resolved shear wave velocity, the stiffness is determined using Equations (2) and (3) above. Stiffness maps depict soft versus stiff tissue regions. Applications of this QUS method, in which linear, elastic, and isotropic tissue behavior is assumed, are presented in Section 3.1.

Many engineered tissues and biomaterials applications (e.g., organ-on-a-chip models, engineered heart valves, engineered skeletal tissues) are thin tissues with thicknesses ranging from 1 mm down to tens of microns. Assessing the stiffness (e.g., elastic modulus) of thin tissues is another promising area of application of USE in the context of regenerative medicine. However, if the spatial extent of the ARF excitation beam is larger than the thickness of the tissue of interest, guided shear waves and dispersive effects impact the estimation of mechanical

properties using USE. In the guided wave phenomenon, the shear wavelength is comparable to the thickness of the thin tissue [9]. During shear wave propagation, waves are guided within the tissue due to reflections against the upper and lower boundaries of the thin layered tissues. Thus, stiffness assessment via shear wave speed using time-domain analysis and Equations (2) and (3) cannot yield accurate results because of the combination of guided wave propagation with shear wave propagation within the layer boundaries of the tissue. In addition, guided wave propagation leads to the separation of the guided wave into its constituent frequency components as it passes through the medium. Analysis of the frequency spectrum of the acquired time domain A-scan signals can be then used to separate guided wave propagation from shear wave propagation. The phase velocity, which is the velocity at which the phase of a single frequency component of the wave travels, can be measured as a function of frequency and fit to analytical solutions [43] to determine the shear modulus of thin soft tissues. In

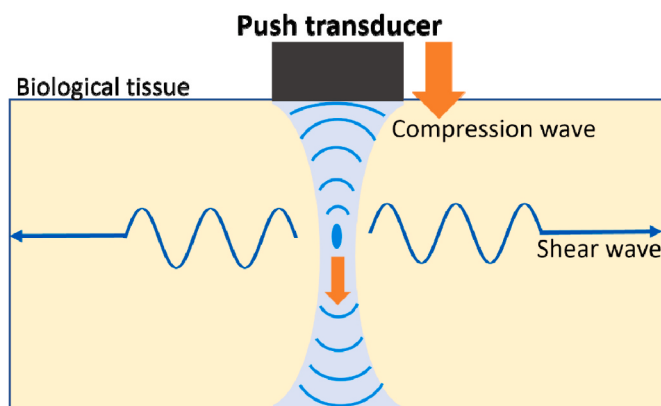


Fig. 4. Depiction of the principles of shear wave propagation whereby acoustic radiation force (via ultrasonic compression waves) produces shear waves (dark blue sinusoidal pulse) that propagate perpendicular to the direction of the force (orange downward arrow) and corresponding outward displacements (dark blue arrow). (For interpretation of the references to color in this figure legend, the reader is referred to the Web version of this article.)

addition, if the phase velocity is dependent on frequency, then the medium is characterized as dispersive. A dispersive medium must be treated as viscoelastic and its corresponding mechanical properties must be determined using a viscoelastic model. In contrast, thick tissues imaged with a spatial extent of the ARF excitation beam larger than the thickness of the tissue (common in clinical applications) lack boundary effects, and thus the effects of dispersion are negligible, and time-domain analysis of shear wave speed can yield accurate estimates of tissue mechanical properties. In general, dispersion is a result of the tissue's thickness, the experimental geometry, and transmission frequency of the excitation. An in-depth discussion of its importance in shear wave propagation is reviewed elsewhere [44].

Using Equation (2), reasonable estimates of mechanical properties of some biological tissues (e.g., breast, liver) are made [42] despite the simplifications used (e.g., linear, elastic, incompressible, and isotropic properties). However, many biological tissues exhibit non-linear, anisotropic, and viscoelastic mechanical behavior (e.g., heart). USE has been applied to assess non-linear elasticity of phantom materials and in organ-level imaging (referred to as nonlinear elasticity imaging and previously reviewed [45]). In non-linear elasticity imaging, US is used to monitor large deformations ($>5\%$ strain) induced in biological tissues where these tissues present a non-linear stress/strain relationship without a permanent change in the microscopic structure. The shear modulus and nonlinear fitting parameters, from various analytical models (e.g., Mooney-Rivlin [46], Veronda-Westmann [47]), can be determined using USE to investigate the nonlinear stress-strain relationships of these materials. For example, Pavan et al. [47], examined the nonlinear elastic behavior of agar and gelatin gels, common phantom materials used in US imaging and found that agar exhibited more non-linear elastic behavior than gelatin. This technique has yet to be applied to engineered tissues or biomaterials to investigate their nonlinear elastic behavior. However, USE has been applied to assess anisotropy and viscoelasticity of engineered tissues and biomaterials. Anisotropy in tissue can be measured using USE by measuring shear wave propagation in different axes. For example, the USE technique that is most used in this context is clinical echocardiography to assess myocardial wall deformation [48] to distinguish between active and passive stiffness of myocardial tissue through measurement of shear wave propagation in the short- and long-axis views [48]. Often, stiffness maps, that are color coded maps that show changes in deformation, before and after application of an ARF, are used in this imaging technique to assess the stiffness of the sample. Anisotropic properties can be assessed using both conventional (Equations (2) and (3)) and phase velocity analysis, depending on the geometric conditions of the tissue. In

viscoelastic materials, a dynamic ARF will create a shear wave, with the wave speed dependent on the material's elastic properties (storage modulus) and the attenuation dependent on its viscous properties (loss modulus). Using phase velocity analysis, the viscoelastic properties of the media can be estimated. Examples of US studies that have assessed viscoelasticity and/or anisotropy in biomaterials and tissues are presented in Section 3.3.2 and 3.3.3.

3. Ultrasound imaging to characterize engineered tissues and scaffolds

The first use of US imaging in TE was first described by Cohn et al. to non-invasively monitor smooth muscle cell proliferation and the Young's modulus of a synthesized tissue layer on 3 mm thick nonwoven arrays made up of polyglycolic acid fibers during culture using an elasticity microscope [49]. This seminal study demonstrated the utility of US for non-invasive assessment of the elastic properties of a synthesized tissue layer in a TE application. Technological developments in both the field of biomedical US imaging and TE provide many applications where the use of non-invasive and non-destructive analyses of engineered tissues and biomaterials would aid in the development of regenerative therapies. US has been used as an analytical tool for this purpose and is described in the following sections. A comprehensive summary including samples studied and their scale, study type, main findings, and limitations is provided in [Supplementary Table 1](#).

3.1. Assessing scaffold degradation longitudinally using ultrasound elastography *in vivo*

Longitudinal evaluation of engineered biomaterials and tissues *in vivo* settings is critical to their assessment and clinical translation. For example, monitoring the kinetics of biomaterial degradation and tissue formation provides important insights into the tissue regeneration process. Conventional US imaging has infrequently been used to evaluate biomaterial degradation; instead, USE is more commonly used to evaluate biomaterial degradation *in vivo* by measuring changes in mechanical parameters (e.g., Young's modulus) as a surrogate measure for degradation. USE is attractive as a clinical imaging modality and well-suited to assess scaffold degradation due to its real-time, non-invasive, and non-destructive capabilities. To this end, Kim et al. first demonstrated *in vivo* use of USE to evaluate poly (1,8-octanediol-co-citrate) cartilage scaffold degradation in a mouse model by measuring changes in scaffold elastic modulus, which they showed correlated with scaffold weight loss [50] (Fig. 5).

Subsequently, USE studies evaluated the degradation of polyurethane-based tissue constructs [51,52] and poly (lactic-co-glycolic acid) phase sensitive *in situ* forming implants [53], and monitored injected gold nanotracer-labeled mesenchymal stem cells in the lower limbs of rats [54].

However, there are limitations to clinical translation of USE in human models for *in vivo* assessment of biomaterials that need to be overcome before widespread adoption. For example, USE requires the ability to apply an external force to a tissue *in vivo* and measure the resultant deformation, which is not possible for all adult human tissues and organs (e.g., adult brain imaging due to the presence of the skull).

3.2. *In vitro* monitoring of the growth, development, and degradation of biomaterials using conventional ultrasound imaging and quantitative ultrasound imaging

The longitudinal assessment of biomaterials *in vitro* is another promising application of US in TE. Although low frequency US imaging is ideal for *in vivo* applications, it is not ideal for *in vitro* applications because its spatial resolution cannot assess functional and mechanical properties on millimeter to micrometer length scales. High frequency US imaging (e.g., >20 MHz) has high spatial resolution (tens of microns)

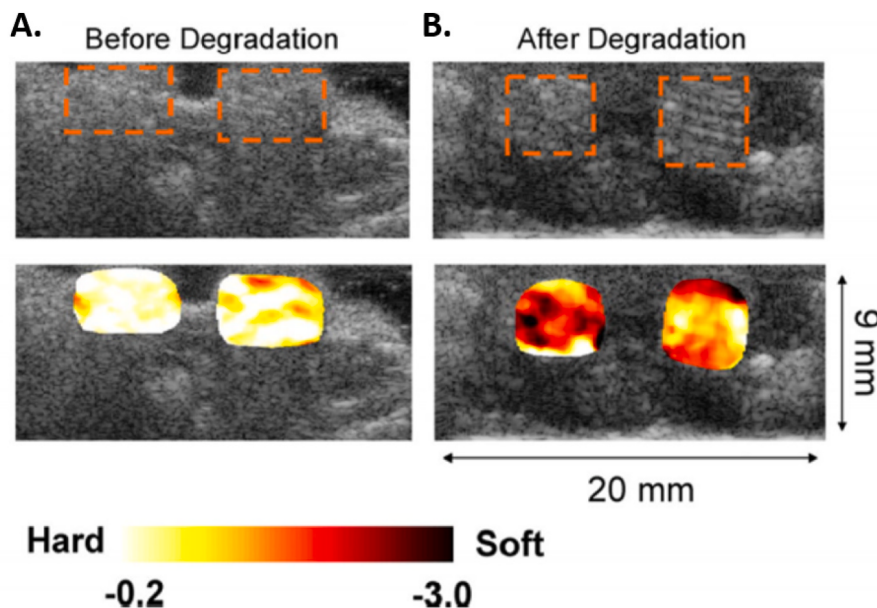


Fig. 5. *In vivo* B-mode USE imaging (defined in Section 2.2.3) of a poly(1,8-octanediol-co-citrate) cartilage (POC) cartilage scaffold degradation in a mouse before (A) and after (B) degradation of the scaffold – adapted from Ref. [50]. Orange square regions in the top row of (A) and (B) show B-mode image regions of interest where the POC cartilage scaffold was implanted. B-mode images in the bottom row of (A) and (B) show overlaid parametric stiffness maps (described in Section 2.2.3) before (A) and after (B) degradation of the POC cartilage scaffold. The color axes represent normalized stiffness values before (A) and after (B) degradation. Figure is adapted from Ref. [50]. (For interpretation of the references to color in this figure legend, the reader is referred to the Web version of this article.)

and low penetration depth (a few millimeters). The trade-off between imaging depth and spatial resolution makes high-frequency US well-suited for *in vitro* studies (e.g., biological systems modeling for disease recapitulation and drug discovery, longitudinal bioreactor analysis, biomaterial growth, development, and degradation evaluation) due its high spatial resolution and limited imaging depth (on the order of the tissue constructs). To this end, to monitor *in vitro* tissue growth, development, and degradation, conventional B-mode US, QUS, and USE techniques have been used. In this section, we focus on conventional B-mode US imaging and Section 3.3 focuses on the use of USE for this application.

Clinical US imaging is widely known for using B-scan images for qualitative assessment in diagnostic evaluations. QUS techniques (described in Section 2.2.1 and 2.2.2) can be applied on A-scan, B-scan, C-scan, and/or M-mode data to assess the acoustic and biological properties of a sample. These techniques have been used to determine the acoustic and biological properties of hydrogels [14,15,30–32,35,37,38,55–62], cartilage [63–66], osteogenic grafts [67,68], and *in situ*

forming implants [69].

QUS techniques that examine frequency-domain characteristics (e.g., spectral parameters) enable characterization of tissue microstructure, such as the number, size, and organization of tissue scatterers. In clinical studies, spectral parameters such as the spectral slope, spectral intercept, and mid-band fit have been used to assess coronary plaque composition [70–72], cardiac tissue necrosis [73,74], disease severity of multiple tissues (e.g., prostate, pancreatic) [75–77] and the response of tumors to treatment [78–80]. Few studies have explored the use of QUS techniques to extract spectral parameters in TE. Preliminary studies have looked at its application in hydrogels constructs [30–32,37,38,55] and demonstrated that quantitative color maps of spectral parameters could measure cell proliferation in a hydrogel scaffold with similar accuracy as quantitative assessment of grayscale pixel analysis in B-mode images. This use of QUS techniques also provided more information about the organization and size of tissue scatterers than grayscale B-mode images [37] (Fig. 6).

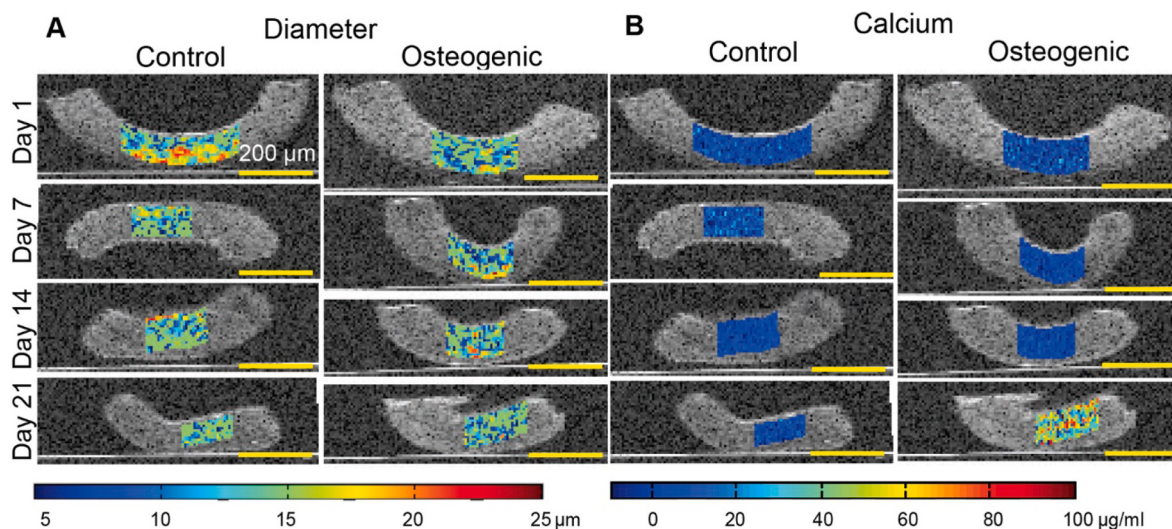


Fig. 6. *In vitro* B-mode images of estimated microstructural parameters (i.e., scatterer diameter (A) and calcium concentration (B)) in tissue constructs during a 21-day culture period. The increase in calcium concentration at Day 21 (B) is indicative of osteogenic differentiation of MC3T3 cells in the constructs – adapted from Ref. [37].

3.3. Ultrasound elastography to evaluate *in vitro* engineered tissues and biomaterials

Although USE has been primarily used for clinical purposes [81], the development of high-frequency US systems with spatial resolutions ranging from 5 to 100 μm enables non-invasive and non-destructive USE spatial mapping of mechanical parameters at the cellular scale. The studies that employ USE to examine the mechanical properties of engineered tissues *in vitro* have considered linear, elastic or viscoelastic, isotropic tissues [82–105]; and anisotropic material behavior in thin tissues [106–110].

3.3.1. Linear, elastic, isotropic tissue property studies

As the field of TE expanded and the application of USE in TE was introduced, USE was used to measure the biomechanical properties of engineered tissues examined cartilage [82,83], tissue-mimicking phantoms [92] (Fig. 7), and 3D cell culture constructs [94–97,101,104]. Generally, these studies used Equations (2) and (3) to determine the Young's modulus of the tissues and validate measurements with atomic force microscopy (AFM), nanoidentation, or tensile testing.

3.3.2. Viscoelastic tissue property studies

Most biological tissues are viscoelastic, exhibiting properties of both elastic solids and viscous fluids. Mauldin Jr. et al. [87] and Liu et al. [88] estimated viscoelastic tissue properties in engineered biomaterials using monitored steady-state excitation and recovering radiation force imaging (MSSER) and ARF imaging (described in Section 2.2.3), respectively. In MSSER, one US linear array transducer with two central frequency beams (6.15 and 4.21 MHz) was used to generate a high-intensity ARF of varying duration (1.4 μs , 1.9 μs , 2.4 μs , 2.9 μs) to track the recovery of thick tissue (>10 mm) to varying magnitudes of applied ARF, from which viscoelastic properties were estimated using Voigt and standard linear viscoelastic models. In the ARF imaging study, a highly focused 5 MHz ARF transducer was used to generate deformation in the tissue paired with a 25 MHz polyvinylidene fluoride imaging transducer to track these displacements in tissue samples on 500 μm thin rigid substrates. Using a second-order forced harmonic oscillator model, they examined the frequency response of the tissue to ARF beams and estimated the viscosity of the samples. However, both of these studies had relatively low axial resolution and low SNR, which hinders their implementation in biological applications of thin tissues.

Most recently, three studies developed USE approaches to assess viscoelastic properties of biomaterials *in vitro* [99–101] with good agreement with mechanical testing, good spatial resolution, and high SNR. Hong et al. developed multi-mode USE systems to investigate the viscoelastic behavior of hydrogels through observation of creep behavior and validated with rheology and nanoindentation [99,100] (Fig. 8). The authors then developed a technique, termed resonant acoustic rheometry, to characterize the viscoelastic mechanical properties of soft hydrogel biomaterials that relied on the frequency

spectrum of the surface acoustic waves detected in the samples via M-mode imaging [101]. Surface acoustic waves are elastic waves that travel at the surface of an elastic material, analogous to shear wave propagation sub-surface. These studies, all evaluated at a microscale, demonstrate the feasibility of US to non-invasively and non-destructively provide accurate measurements of viscoelastic properties with high spatial resolution in engineering biomaterials. However, these techniques are limited by the focal properties of the excitation and detection transducer. For example, the axial resolution in these studies was not sufficient to assess small, thin (<1 mm) tissues.

3.3.3. Anisotropic and/or thin tissue property studies

In clinical USE systems with limited spatial resolution, the effects of guided shear waves prohibit stiffness assessment using time-domain analysis of acquired US signals and Equations (2) and (3) (described in Section 2.2.3). Past studies have examined the mechanical properties of thin soft tissues using guided wave elastography (GWE), including the arterial wall [43], cornea [106], heart wall [107], bladder wall [108], and Achilles' tendon [109]. The method to assess the Achilles' tendon is depicted in Fig. 9. Recently, Li et al. presented an inverse approach based on the dispersion relation of guided waves in a layered structure to quantitatively measure the elastic properties of multi-layered thin tissues [90]. This GWE approach can extend to multi-layered biological tissues (e.g., skeletal tissue, connective tissue, and blood vessels) [110] to determine the dispersion relation but has yet to be implemented for biomaterial assessment.

4. Future perspectives on ultrasound imaging to characterize engineered tissues

Although many studies have examined the use of US in TE applications, there are many avenues still to be explored.

4.1. Ultrafast ultrasound imaging to evaluate engineered biomaterials and replacement tissues clinically

Ultrafast ultrasound imaging is a novel imaging method that is able to capture images at frame rates up to 100 times faster than conventional *in vivo* imaging methods (up to 5000 frames per second). It has most commonly been used in *in vivo* applications such as blood flow imaging [111], transcranial imaging [112], and myocardial stiffness assessment [113]. Of note, ultrafast ultrasound has shown its excellent ability to estimate the stiffness of tissue at a patient's bedside [114,115], and its high temporal resolution would enable simultaneous imaging of rapid organ and/or tissue movements (e.g., heart contractions), and elastographic visualization of biomaterial degradation kinetics at a temporal scale that cannot be reached by conventional *in vivo* ultrasound techniques [50,51,53]. Depending on the application and the tissues or materials' properties, different types of acoustic techniques can be used using ultrafast ultrasound. Shear wave mapping, that obtains a stiffness

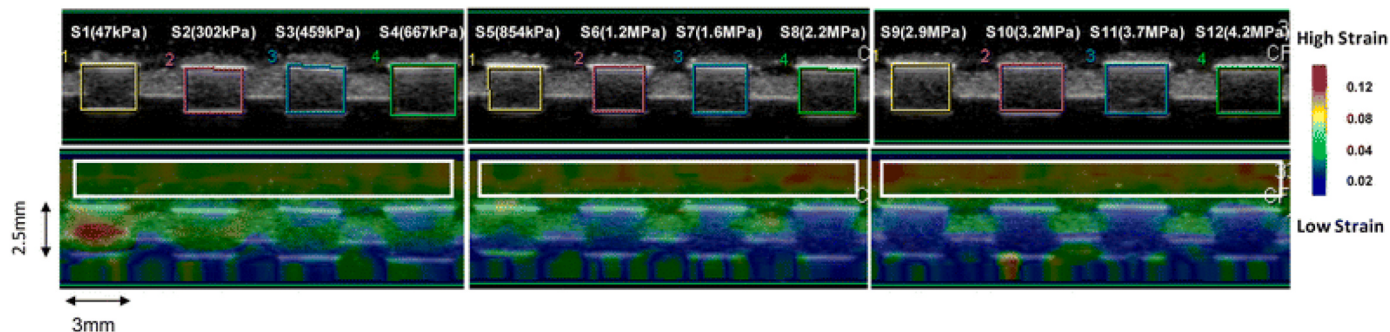


Fig. 7. B-mode images (top row) and superimposed strain maps (bottom row) of PDMS samples embedded in polyacrylamide tissue mimicking phantoms. A decrease in strain is observed with increasing modulus from left (sample 1) to right (sample 12). Figure taken from Ref. [86].

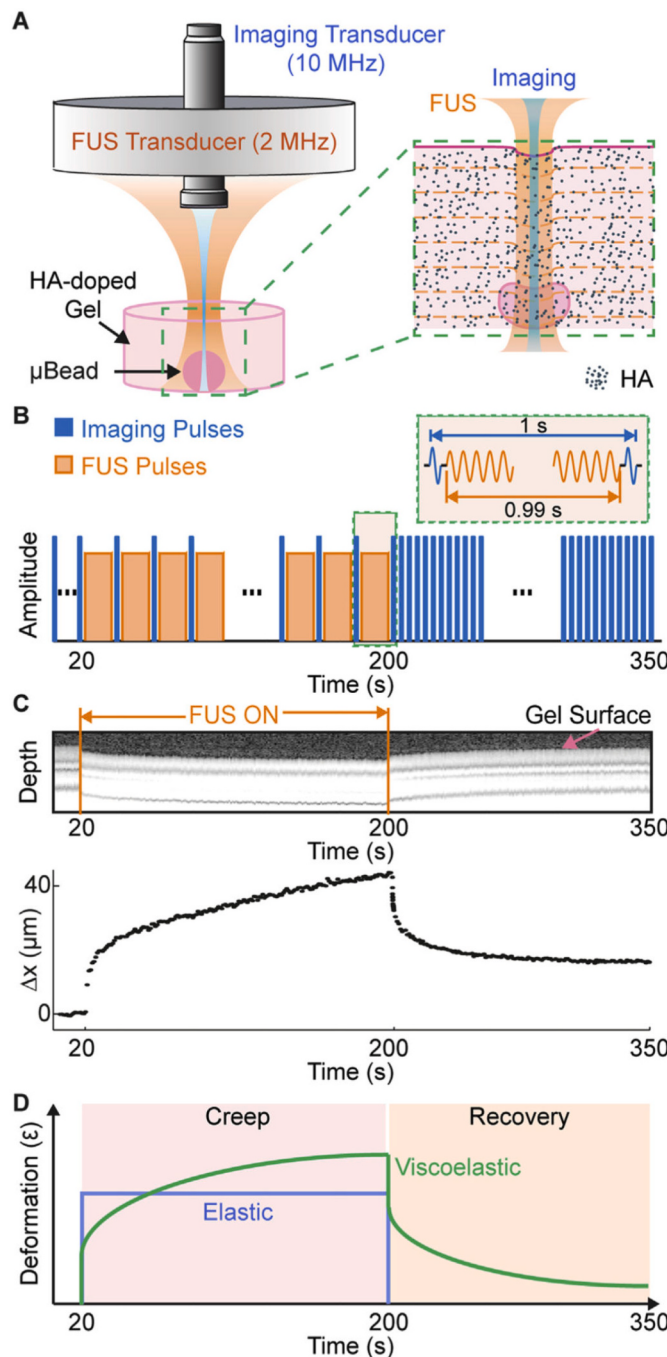


Fig. 8. Multi-mode US viscoelastography with focused US (FUS) in hydroxyapatite (HA) doped gels with embedded HA-agarose beads (μ Beads) from Ref. [100] with (A) the experimental schematic, (B) excitation and detection sequences, (C) M-mode grayscale image with respective peak displacement-time curve of an agarose gel showing deformation and (D) conceptual schematic of deformation-time curves for elastic and viscoelastic materials.

map, can be performed on a relatively homogeneous and anisotropic static sample. If an engineered tissue or biomaterial was implanted on or close to a moving organ or tissue, iterative approaches of localized ARF or natural shear wave assessment are required [111]. Despite the technical differences, the general idea is the same: to study shear wave velocity to deduce tissue stiffness and an elastic modulus [116]. In addition to stiffness assessment, ultrafast ultrasound imaging allows exploration and analysis of the fiber orientation of a biological tissue or material using 3D ultrasound backscatter tensor imaging [117]. By leveraging the

high spatiotemporal coherence of backscattered echoes at each point of a section (in 2D) or a volume (in 3D), the fiber orientation can be deduced. Implementation of this technique would enable the examination of the effects of engineered biomaterials anisotropic structural properties on their longitudinal efficacy post-implantation or degradation kinetics.

4.2. Acoustic biomicroscopy to evaluate contractility in cell and 3D tissue models

Several types of cells exhibit contractile behavior, including cardiomyocytes, skeletal and smooth muscle cells, and myofibroblasts, both in 2D culture and in 3D engineered tissues. Contractility is an important metric for evaluating the health, maturation, and pathophysiology of cellular function, but is not a routine assay due to the lack of easy to use, non-invasive contractile assessment tools [118]. To address this need, we developed high-frequency US to assess the contractility of cells and tissues non-invasively, non-destructively, and label-free, with temporal resolutions better than 1000 frames per second [119]. In this approach, US was used to measure deformation of contracting single cardiomyocytes or 3D microtissues with high precision using single-element transducers. This is a highly versatile method, able to measure contractility in a wide range of common *in vitro* configurations without the need for specialized well plates or substrates. Importantly, the high temporal resolution of acoustic biomicroscopy enabled high fidelity imaging of beat kinetics and aberrant beat characteristics that are missed with conventional lower speed optical-based measurements. Contractile force was also reliably estimated with this approach, but required independent measurement of the cell elastic modulus. Future development of this method could address this limitation with USE (Section 4.3) to provide a fully-integrated system for contractile force measurement.

4.3. Ultrasound elastography to estimate the biomechanical properties of thin engineered tissues, organs-on-a-chip, and organoids

Predicting the effects of drugs before human clinical trials is fundamental to the drug screening and discovery process [120]. However, current drug screening and testing methods (e.g., two-dimensional cell culture models, animal models) lack the predictive power to eliminate ineffective drug candidates [121,122]. Organoid and organ-on-a-chip (OOAC) models incorporating 3D engineered microtissues and human induced pluripotent stem cells show great promise to better mimic *in vivo* human biology, disease, and drug responses [123,124]. Organoid and OOAC models of disease pathology include cardiac fibrosis [125], congenital heart disease [126], muscular dystrophy [127], liver fibrosis [128], breast cancer [129], and pulmonary fibrosis [130], to name a few. Of the many biomarkers available to assess disease pathogenesis, change in tissue stiffness is one indicator of disease and drug toxicity in some cases [131]. Current measurement techniques (e.g., atomic force microscopy, nanoindentation, tensile testing) are well-established to measure stiffness in these applications; however, these approaches are invasive and incapable of monitoring engineered tissue stiffness over time in culture as they are performed *ex situ*. As mentioned in Section 3.3, USE is a non-invasive, non-destructive technique theoretically capable of assessing the longitudinal stiffness of engineered tissues undergoing drug treatment in disease models. However, as organoids and OOAC models are manufactured on the millimeter to sub-millimeter scale, high-frequency USE must be used to achieve sufficient spatial resolution to deduce the stiffness of the sample (Section 2.1.2). In addition, frequency-dependent attenuation must also be considered to generate sufficient ARF to create elastic waves in the sample of interest (Section 2.1.1). Generally, the single-element transducers and systems used in these applications will need to be custom-made with the disease application and model size specifications in mind, since commercial systems and transducers do not have the design requirements necessary

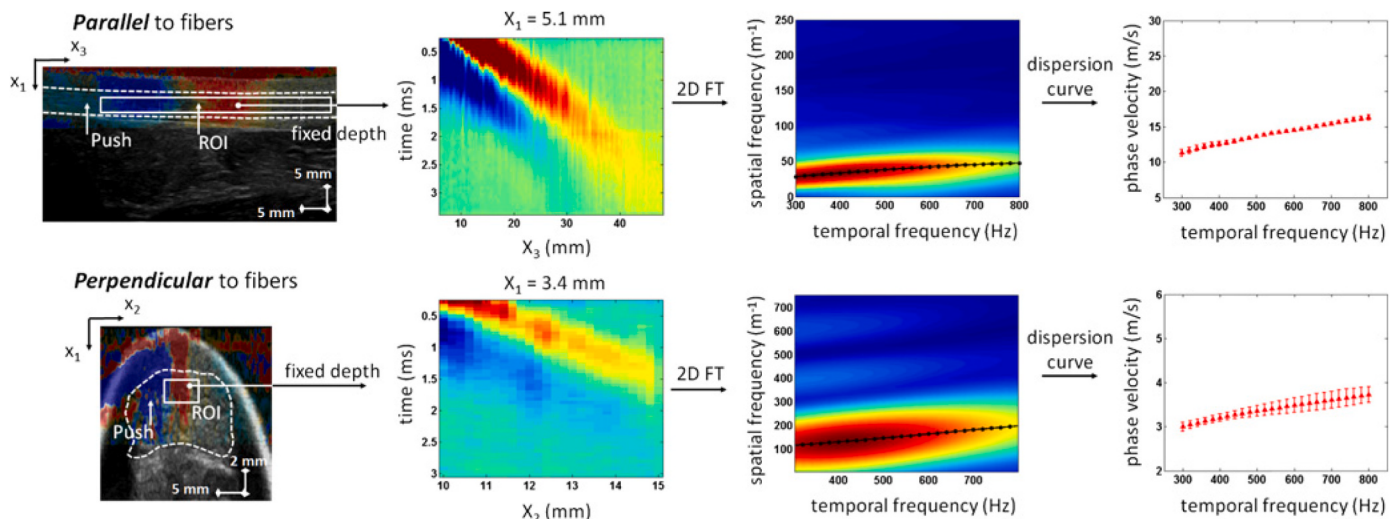


Fig. 9. Achilles tendon analysis using shear wave elastography using B-mode imaging (left-most panel), displacement mapping (middle-left panel), k-space analysis (right-most panel). The top row is parallel to fibers and bottom row is perpendicular to fibers. Figure taken from Ref. 109.

to assess these properties.

5. Conclusions

Ultrasound imaging enables non-invasive, non-destructive, real-time, longitudinal, and quantitative assessment of biomaterial, cell, and tissue properties that are relevant for *in vivo* applications in tissue engineering, translational biomaterials research, and regenerative medicine. Emerging advances in high frequency ultrasound imaging are further extending its capabilities to enable *in vitro* quantitative assessment of cell and tissue microstructure, function, and mechanics at centimeter to sub-micron length scales. These innovations open up new opportunities for ultrasound imaging, including promising applications in monitoring and assessment of organoids, microtissues, and organ-on-a-chip models used in basic science and drug development and testing.

Declaration of competing interest

The authors declare that they have no known competing financial interests or personal relationships that could have appeared to influence the work reported in this paper.

Data availability

No data was used for the research described in the article.

Appendix A. Supplementary data

Supplementary data to this article can be found online at <https://doi.org/10.1016/j.biomaterials.2023.122054>.

References

- [1] D. Dalecki, D.C. Hocking, Advancing ultrasound technologies for tissue engineering, in: *Handbook of Ultrasonics and Sonochemistry*, Springer Singapore, 2016, pp. 1101–1126, https://doi.org/10.1007/978-981-287-278-4_28.
- [2] K. Kim, W.R. Wagner, Non-invasive and non-destructive characterization of tissue engineered constructs using ultrasound imaging technologies: a review, *Ann. Biomed. Eng.* 44 (3) (2016) 621–635, <https://doi.org/10.1007/s10439-015-1495-0>.
- [3] D. Dalecki, K.P. Mercado, D.C. Hocking, Quantitative ultrasound for nondestructive characterization of engineered tissues and biomaterials, *Ann. Biomed. Eng.* 44 (3) (2016) 636–648, <https://doi.org/10.1007/s10439-015-1515-0>.
- [4] C.X. Deng, X. Hong, J.P. Stegemann, Ultrasound imaging techniques for spatiotemporal characterization of composition, microstructure, and mechanical properties in tissue engineering, *Tissue Eng. B Rev.* 22 (4) (2016) 311–321, <https://doi.org/10.1089/ten.teb.2015.0453>.
- [5] D. Dalecki, D.C. Hocking, Ultrasound technologies for biomaterials fabrication and imaging, *Ann. Biomed. Eng.* 43 (3) (2015) 747–761, <https://doi.org/10.1007/s10439-014-1158-6>.
- [6] U.K.M. Teichgräber, J.M.A. Meyer, C.P. Nautrup, D.B. Rautenfeld, Ultrasound anatomy: a practical teaching system in human gross anatomy, *Med. Educ.* 30 (4) (1996) 296–298, <https://doi.org/10.1111/j.1365-2923.1996.tb00832.x>.
- [7] E. Macé, G. Montaldo, I. Cohen, M. Baulac, M. Fink, M. Tanter, Functional ultrasound imaging of the brain, *Nat. Methods* 8 (8) (2011) 662–664, <https://doi.org/10.1038/nmeth.1641>.
- [8] K.G. Baker, V.J. Robertson, F.A. Duck, A review of therapeutic ultrasound: biophysical effects, *Phys. Ther.* 81 (7) (2001) 1351–1358, <https://doi.org/10.1093/pjt/81.7.1351>.
- [9] R.S.C. Cobbold, *Foundations of Biomedical Ultrasound*, Oxford University Press, 2007.
- [10] F.A. Duck, Acoustic properties of tissue at ultrasonic frequencies, in: *Physical Properties of Tissues*, Elsevier, 1990, pp. 73–135, <https://doi.org/10.1016/B978-0-12-222800-1.50008-5>.
- [11] F.T. D'Astous, F.S. Foster, Frequency dependence of ultrasound attenuation and backscatter in breast tissue, *Ultrasound Med. Biol.* 12 (10) (1986) 795–808, [https://doi.org/10.1016/0301-5629\(86\)90077-3](https://doi.org/10.1016/0301-5629(86)90077-3).
- [12] I.Z. Nenadic, B. Qiang, M.W. Urban, H. Zhao, W. Sanchez, J.F. Greenleaf, S. Chen, Attenuation measuring ultrasound shearwave elastography and *in vivo* application in post-transplant liver patients, *Phys. Med. Biol.* 62 (2) (2017) 484–500, <https://doi.org/10.1088/1361-6560/aa4f6f>.
- [13] K. Nam, I.M. Rosado-Mendez, L.A. Wirtzfeld, A.D. Pawlicki, V. Kumar, E. L. Madsen, G. Ghoshal, R.J. Lavarello, M.L. Oelze, T.A. Bigelow, J.A. Zagzebski, W.D. O'Brien, T.J. Hall, Ultrasonic attenuation and backscatter coefficient estimates of rodent-tumor-mimicking structures: comparison of results among clinical scanners, *Ultrason. Imag.* 33 (4) (2011) 233–250, <https://doi.org/10.1177/016173461103300403>.
- [14] A. Ruland, J.M. Hill, G.G. Wallace, Reference phantom method for ultrasonic imaging of thin dynamic constructs, *Ultrasound Med. Biol.* 47 (8) (2021) 2388–2403, <https://doi.org/10.1016/j.ultrasmedbio.2021.04.014>.
- [15] J.A. Sebastian, E.M. Strohm, E. Chérin, B. Mirani, C. Démoré, M.C. Kolios, C. A. Simmons, High-frequency quantitative ultrasound for the assessment of the acoustic properties of engineered tissues *in vitro*, *Acta Biomater.* (2022), <https://doi.org/10.1016/j.actbio.2022.12.014>. S1742706122008170.
- [16] C.R. Hill, J.C. Bamber, G. ter Haar (Eds.), *Physical Principles of Medical Ultrasonics*, second ed., John Wiley & Sons, 2004.
- [17] J.C. Bamber, C. Daft, Adaptive filtering for reduction of speckle in ultrasonic pulse-echo images, *Ultrasonics* 24 (1) (1986) 41–44, [https://doi.org/10.1016/0041-624X\(86\)90072-7](https://doi.org/10.1016/0041-624X(86)90072-7).
- [18] J.C. Bamber, Speckle reduction, ch. 5, in: P.N.T. Wells (Ed.), *Advances in Ultrasound Techniques and Instrumentation (Clinics in Diagnostic Ultrasound)*, vol. 28, Churchill Livingstone, New York, 1993, pp. 55–67.
- [19] M. Kolios, Biomedical ultrasound imaging from 1 to 1000 MHz, *Canadian Acoustics [Internet]* 37 (3) (2009 Sep. 1) 35–43. <https://jcaa.caa-aca.ca/index.php/jcaa/article/view/2124>.
- [20] J. Mamou, M.L. Oelze (Eds.), *Quantitative Ultrasound in Soft Tissues*, Springer, Dordrecht, 2013.

- [21] T.L. Szabo, Diagnostic Ultrasound Imaging: inside Out, Elsevier Academic Press, 2004.
- [22] K. Nam, J.A. Zagzebski, T.J. Hall, Simultaneous backscatter and attenuation estimation using a least squares method with constraints, *Ultrasound Med. Biol.* 37 (2011) 2096–2104, <https://doi.org/10.1016/j.ultrasmedbio.2011.08.008>.
- [23] K. Nam, I.M. Rosado-Mendez, L.A. Wirtzfeld, V. Kumar, E.L. Madsen, G. Ghoshal, A.D. Pawlicki, M.L. Oelze, R.J. Lavarello, T.A. Bigelow, J.A. Zagzebski, W. D. O'Brien, T.J. Hall, Cross-imaging system comparison of backscatter coefficient estimates from a tissue-mimicking material, *J. Acoust. Soc. Am.* 132 (2012) 1319–1324, <https://doi.org/10.1121/1.4742725>.
- [24] K. Nam, I.M. Rosado-Mendez, L.A. Wirtzfeld, A.D. Pawlicki, V. Kumar, E. L. Madsen, G. Ghoshal, R.J. Lavarello, M.L. Oelze, T.A. Bigelow, J.A. Zagzebski, W.D. O'Brien, T.J. Hall, Ultrasonic attenuation and backscatter coefficient estimates of rodent-tumor-mimicking structures: comparison of results among clinical scanners, *Ultras. Imag.* 33 (2011) 233–250, <https://doi.org/10.1177/01617346110300403>.
- [25] J.J. Anderson, M.-T. Herd, M.R. King, A. Haak, Z.T. Hafez, J. Song, M.L. Oelze, E. L. Madsen, J.A. Zagzebski, W.D. O'Brien, T.J. Hall, Interlaboratory comparison of backscatter coefficient estimates for tissue-mimicking phantoms, *Ultras. Imag.* 32 (2010) 48–64, <https://doi.org/10.1177/016173461003200104>.
- [26] F.T. D'Astous, F.S. Foster, Frequency dependence of ultrasound attenuation and backscatter in breast tissue, *Ultrasound Med. Biol.* 12 (1986) 795–808, [https://doi.org/10.1016/0301-5629\(86\)90077-3](https://doi.org/10.1016/0301-5629(86)90077-3).
- [27] J. Mamou, A. Coron, M.L. Oelze, E. Saegusa-Beecroft, M. Hata, P. Lee, J. Machi, E. Yanagihara, P. Laugier, E.J. Feleppa, Three-dimensional high-frequency backscatter and envelope quantification of cancerous human lymph nodes, *Ultrasound Med. Biol.* 37 (2011) 345–357, <https://doi.org/10.1016/j.ultrasmedbio.2010.11.020>.
- [28] Z. Vered, G.A. Mohr, B. Barzilai, C.J. Gessler, S.A. Wickline, K.A. Wear, T. A. Shoup, A.N. Weiss, B.E. Sobel, J.G. Miller, J.E. Perez, Ultrasound integrated backscatter tissue characterization of remote myocardial infarction in human subjects, *J. Am. Coll. Cardiol.* 13 (1989) 84–91, [https://doi.org/10.1016/0735-1097\(89\)90553-6](https://doi.org/10.1016/0735-1097(89)90553-6).
- [29] C.M. Moran, N.L. Bush, J.C. Bamber, Ultrasonic propagation properties of excised human skin, *Ultrasound Med. Biol.* 21 (1995) 1177–1190, [https://doi.org/10.1016/0301-5629\(95\)00049-6](https://doi.org/10.1016/0301-5629(95)00049-6).
- [30] A. Ruland, K.J. Gilmore, L.Y. Daikuara, C.D. Fay, Z. Yue, G.G. Wallace, Quantitative ultrasound imaging of cell-laden hydrogels and printed constructs, *Acta Biomater.* 91 (2019) 173–185, <https://doi.org/10.1016/j.actbio.2019.04.055>.
- [31] K.P. Mercado, M. Helguera, D.C. Hocking, D. Dalecki, Noninvasive quantitative imaging of collagen microstructure in three-dimensional hydrogels using high-frequency ultrasound, *Tissue Eng. C Methods* 21 (2015) 671–682, <https://doi.org/10.1089/ten.tec.2014.0527>.
- [32] K.P. Mercado, M. Helguera, D.C. Hocking, D. Dalecki, Estimating cell concentration in three-dimensional engineered tissues using high frequency quantitative ultrasound, *Ann. Biomed. Eng.* 42 (6) (2014) 1292–1304, <https://doi.org/10.1007/s10439-014-0994-8>.
- [33] M.P. Moore, T. Spencer, D.M. Salter, P.P. Kearney, T.R. Shaw, I.R. Starkey, P. J. Fitzgerald, R. Erbel, A. Lange, N.W. McDicken, G.R. Sutherland, K.A. Fox, Characterisation of coronary atherosclerotic morphology by spectral analysis of radiofrequency signal: in vitro intravascular ultrasound study with histological and radiological validation, *Heart* 79 (1998) 459–467, <https://doi.org/10.1136/hrt.79.5.459>.
- [34] C. Lin, L. Cao, J. Wang, W. Zheng, Y. Chen, Z. Feng, A. Li, J. Zhou, Ultrasonic spectrum analysis for *in vivo* characterization of tumor microstructural changes in the evaluation of tumor response to chemotherapy using diagnostic ultrasound, *BMC Cancer* 13 (2013) 302, <https://doi.org/10.1186/1471-2407-13-302>.
- [35] M. Gudur, R.R. Rao, Y.-S. Hsiao, A.W. Peterson, C.X. Deng, J.P. Stegemann, Noninvasive, quantitative, spatiotemporal characterization of mineralization in three-dimensional collagen hydrogels using high-resolution spectral ultrasound imaging, *Tissue Eng. C Methods* 18 (12) (2012) 935–946, <https://doi.org/10.1089/ten.tec.2012.0180>.
- [36] M.C. Kolios, G.J. Czarnota, M. Lee, J.W. Hunt, M.D. Sherar, Ultrasonic spectral parameter characterization of apoptosis, *Ultrasound Med. Biol.* 28 (5) (2002) 589–597, [https://doi.org/10.1016/S0301-5629\(02\)00492-1](https://doi.org/10.1016/S0301-5629(02)00492-1).
- [37] M.S.R. Gudur, R.R. Rao, A.W. Peterson, D.J. Caldwell, J.P. Stegemann, C.X. Deng, Noninvasive quantification of *In vitro* osteoblastic differentiation in 3D engineered tissue constructs using spectral ultrasound imaging, *PLoS One* 9 (2014), e85749, <https://doi.org/10.1371/journal.pone.0085749>.
- [38] G.G. Bushnell, X. Hong, R.M. Hartfield, Y. Zhang, R.S. Oakes, S.S. Rao, J.S. Jeruss, J.P. Stegemann, C.X. Deng, L.D. Shea, High frequency spectral ultrasound imaging to detect metastasis in implanted biomaterial scaffolds, *Ann. Biomed. Eng.* 48 (1) (2020) 477–489, <https://doi.org/10.1007/s10439-019-02366-2>.
- [39] K. Nightingale, M.S. Soo, R. Nightingale, G. Trahey, Acoustic radiation force impulse imaging: *in vivo* demonstration of clinical feasibility, *Ultrasound Med. Biol.* 28 (2002) 227–235, [https://doi.org/10.1016/S0301-5629\(01\)00499-9](https://doi.org/10.1016/S0301-5629(01)00499-9).
- [40] A.P. Sarvazyan, O.V. Rudenko, S.D. Swanson, J.B. Fowlkes, S.Y. Emelianov, Shear wave elasticity imaging: a new ultrasonic technology of medical diagnostics, *Ultrasound Med. Biol.* 24 (1998) 1419–1435, [https://doi.org/10.1016/S0301-5629\(98\)00110-0](https://doi.org/10.1016/S0301-5629(98)00110-0).
- [41] J. Bercoff, M. Tanter, M. Fink, Supersonic shear imaging: a new technique for soft tissue elasticity mapping, *IEEE Trans. Ultrason. Ferroelectrics Freq. Control* 51 (2004) 396–409, <https://doi.org/10.1109/TUFFC.2004.1295425>.
- [42] I.Z. Nenadic (Ed.), Handbook of Ultrasound Elastography: Biomedical Applications and Medicine, Wiley, 2018.
- [43] M. Couade, M. Pernot, C. Prada, E. Messas, J. Emmerich, P. Bruneval, A. Criton, M. Fink, M. Tanter, Quantitative assessment of arterial wall biomechanical properties using shear wave imaging, *Ultrasound Med. Biol.* 36 (10) (2010) 1662–1676, <https://doi.org/10.1016/j.ultrasmedbio.2010.07.004>.
- [44] H. Li, G. Flé, M. Bhatt, Z. Qu, S. Ghazavi, L. Yazdani, G. Bosio, I. Rafati, G. Cloutier, Viscoelasticity imaging of biological tissues and single cells using shear wave propagation, *Frontiers in Physics* 9 (2021), 666192, <https://doi.org/10.3389/fphy.2021.666192>.
- [45] J. Hall, T.E. Barbone, P.A. Oberai, A. J. Jiang, J.-F. Dord, S. Goenezen, G. Fisher, T. Recent results in nonlinear strain and modulus imaging, *Curr. Med. Imag. Rev.* 7 (4) (2011) 313–327, <https://doi.org/10.2174/157340511798038639>.
- [46] R.Q. Erkamp, A.R. Skovoroda, S.Y. Emelianov, M. O'Donnell, Measuring the nonlinear elastic properties of tissue-like phantoms, *IEEE Trans. Ultrason. Ferroelectrics Freq. Control* 51 (4) (April 2004) 410–419, <https://doi.org/10.1109/TUFFC.2004.1295426>.
- [47] T.Z. Pavan, E.L. Madsen, G.R. Frank, A. Adilton O Carneiro, T.J. Hall, Nonlinear elastic behavior of phantom materials for elastography, *Phys. Med. Biol.* 55 (9) (2010) 2679–2692, <https://doi.org/10.1088/0031-9155/55/9/017>.
- [48] J.C. Villalobos Lizardi, J. Baranger, M.B. Nguyen, A. Asnacios, A. Malik, J. Lumens, L. Mertens, M.K. Friedberg, C.A. Simmons, M. Pernot, O. Villemain, A guide for assessment of myocardial stiffness in health and disease, *Nature Cardiovascular Research* 1 (1) (2022) 8–22, <https://doi.org/10.1038/s44161-021-00007-3>.
- [49] N. Abraham Cohn, B.-S. Kim, R.Q. Erkamp, D.J. Mooney, S.Y. Emelianov, A. R. Skovoroda, M. O'Donnell, High-resolution elasticity imaging for tissue engineering, *IEEE Trans. Ultrason. Ferroelectrics Freq. Control* 47 (2000) 956–966, <https://doi.org/10.1109/58.852079>.
- [50] K. Kim, C.G. Jeong, S.J. Hollister, Non-invasive monitoring of tissue scaffold degradation using ultrasound elasticity imaging, *Acta Biomater.* 4 (4) (2008) 783–790, <https://doi.org/10.1016/j.actbio.2008.02.010>.
- [51] J. Yu, K. Takanari, Y. Hong, K.-W. Lee, N.J. Amoroso, Y. Wang, W.R. Wagner, K. Kim, Non-invasive characterization of polyurethane-based tissue constructs in a rat abdominal repair model using high frequency ultrasound elasticity imaging, *Biomaterials* 34 (11) (2013) 2701–2709, <https://doi.org/10.1016/j.biomaterials.2013.01.036>.
- [52] D.W. Park, S.-H. Ye, H.B. Jiang, D. Dutta, K. Nonaka, W.R. Wagner, K. Kim, In vivo monitoring of structural and mechanical changes of tissue scaffolds by multimodality imaging, *Biomaterials* 35 (27) (2014) 7851–7859, <https://doi.org/10.1016/j.biomaterials.2014.05.088>.
- [53] H. Zhou, A. Gawlik, C. Hernandez, M. Goss, J. Mansour, A. Exner, Nondestructive characterization of biodegradable polymer erosion *in vivo* using ultrasound elastography imaging, *ACS Biomater. Sci. Eng.* 2 (6) (2016) 1005–1012, <https://doi.org/10.1021/acsbiomaterials.6b00128>. Scopus.
- [54] S.Y. Nam, L.M. Ricles, L.J. Suggs, S.Y. Emelianov, In vivo ultrasound and photoacoustic monitoring of mesenchymal stem cells labeled with gold nanotracers, *PLoS One* 7 (5) (2012), e37267, <https://doi.org/10.1371/journal.pone.0037267>.
- [55] A. Ruland, C. Onofrillo, S. Duchi, C. Di Bella, G.G. Wallace, Standardised quantitative ultrasound imaging approach for the contact-less three-dimensional analysis of neocartilage formation in hydrogel-based bioscaffolds, *Acta Biomater.* 147 (2022) 129–146, <https://doi.org/10.1016/j.actbio.2022.05.037>.
- [56] K.P. Mercado, M. Helguera, D.C. Hocking, D. Dalecki, Estimating cell concentration in three-dimensional engineered tissues using high frequency quantitative ultrasound, *Ann. Biomed. Eng.* 42 (2014) 1292–1304, <https://doi.org/10.1007/s10439-014-0994-8>.
- [57] A. Cafarelli, A. Verbeni, A. Poliziani, P. Dario, A. Menciassi, L. Ricotti, Tuning acoustic and mechanical properties of materials for ultrasound phantoms and smart substrates for cell cultures, *Acta Biomater.* 49 (2017) 368–378, <https://doi.org/10.1016/j.actbio.2016.11.049>.
- [58] M. Aliabouzar, G.L. Zhang, K. Sarkar, Acoustic and mechanical characterization of 3D-printed scaffolds for tissue engineering applications, *Biomed. Mater.* 13 (2018), 055013, <https://doi.org/10.1088/1748-605X/aad417>.
- [59] M. Rice, K. Waters, K. Anseth, Ultrasound monitoring of cartilaginous matrix evolution in degradable PEG hydrogels, *Acta Biomater.* 5 (2009) 152–161, <https://doi.org/10.1016/j.actbio.2008.07.036>.
- [60] J.M. Walker, A.M. Myers, M.D. Schluchter, V.M. Goldberg, A.I. Caplan, J. A. Berilla, J.M. Mansour, J.F. Welter, Nondestructive evaluation of hydrogel mechanical properties using ultrasound, *Ann. Biomed. Eng.* 39 (2011) 2521–2530, <https://doi.org/10.1007/s10439-011-0351-0>.
- [61] S. Kreitz, G. Dohmen, S. Hasken, T. Schmitz-Rode, P. Melo, S. Jockenhoevel, Nondestructive method to evaluate the collagen content of fibrin-based tissue engineered structures via ultrasound, *Tissue Eng. C Methods* 17 (10) (2011) 1021–1026, <https://doi.org/10.1089/ten.tec.2010.0669>.
- [62] R.C. Gessner, A.D. Hanson, S. Feingold, A.T. Cashion, A. Corcimaru, B.T. Wu, C. R. Mullins, S.R. Aylward, L.M. Reid, P.A. Dayton, Functional ultrasound imaging for assessment of extracellular matrix scaffolds used for liver organoid formation, *Biomaterials* 34 (37) (2013) 9341–9351, <https://doi.org/10.1016/j.biomaterials.2013.08.033>.
- [63] J.M. Walker, A.M. Motavalli, J.E. Dennis, T.J. Kean, A.I. Caplan, J.A. Berilla, J. F. Welter, Rapid detection of shear-induced damage in tissue-engineered cartilage using ultrasound, *Tissue Eng. C Methods* 24 (2018) 443–456, <https://doi.org/10.1089/ten.tec.2017.0513>.
- [64] Y. Tanaka, Y. Saito, Y. Fujihara, H. Yamaoka, S. Nishizawa, S. Nagata, T. Ogasawara, Y. Asawa, T. Takato, K. Hoshi, Evaluation of the implant type tissue-engineered cartilage by scanning acoustic microscopy, *J. Biosci. Bioeng.* 113 (2012) 252–257, <https://doi.org/10.1016/j.jbiosc.2011.10.011>.

- [65] Y. Sun, D. Responde, H. Xie, J. Liu, H. Fatakdawala, J. Hu, K.A. Athanasiou, L. Marcu, Nondestructive evaluation of tissue engineered articular cartilage using time-resolved fluorescence spectroscopy and ultrasound backscatter microscopy, tissue engineering Part C, Methods 18 (2012) 215–226, <https://doi.org/10.1089/ten.tec.2011.0343>.
- [66] B.Z. Fite, M. Decaris, Y. Sun, Y. Sun, A. Lam, C.K.L. Ho, J.K. Leach, L. Marcu, Noninvasive multimodal evaluation of bioengineered cartilage constructs combining time-resolved fluorescence and ultrasound imaging, Tissue Eng. C Methods 17 (2011) 495–504, <https://doi.org/10.1089/ten.tec.2010.0368>.
- [67] J. Melchor, E. López-Ruiz, J. Soto, G. Jiménez, C. Antich, M. Perán, J.M. Baena, J. A. Marchal, G. Rus, In-bioreactor ultrasonic monitoring of 3D culture human engineered cartilage, Sensor. Actuator. B Chem. 266 (2018) 841–852, <https://doi.org/10.1016/j.snb.2018.03.152>.
- [68] J.N. Harvestine, C.S. Sheaff, C. Li, A.K. Haudenschild, M.A. Gionet-Gonzales, J. C. Hu, K.A. Athanasiou, L. Marcu, J.K. Leach, Multimodal label-free imaging for detecting maturation of engineered osteogenic grafts, ACS Biomater. Sci. Eng. 5 (2019) 1956–1966, <https://doi.org/10.1021/acsbiomaterials.9b00007>.
- [69] L. Solorio, B.M. Babin, R.B. Patel, J. Mach, N. Azar, A.A. Exner, Noninvasive characterization of in situ forming implants using diagnostic ultrasound, J. Contr. Release 143 (2) (2010) 183–190, <https://doi.org/10.1016/j.jconrel.2010.01.001>.
- [70] K. Nasu, E. Tsuchikane, O. Katoh, D.G. Vince, R. Virmani, J.-F. Sturney, A. Murata, Y. Takeda, T. Ito, M. Ehara, T. Matsubara, M. Terashima, T. Suzuki, Accuracy of *In vivo* coronary plaque morphology assessment, J. Am. Coll. Cardiol. 47 (2006) 2405–2412, <https://doi.org/10.1016/j.jacc.2006.02.044>.
- [71] A. Nair, B.D. Kuban, E.M. Tuzcu, P. Schoenhagen, S.E. Nissen, D.G. Vince, Coronary plaque classification with intravascular ultrasound radiofrequency data analysis, Circulation 106 (2002) 2200–2206, <https://doi.org/10.1161/01.CIR.0000035654.18341.5E>.
- [72] J. Qian, A. Maehara, G.S. Mintz, M.P. Margolis, A. Lerman, J. Rogers, S. Banai, S. Kazziha, C. Castellanos, L. Dani, M. Fahy, G.W. Stone, M.B. Leon, Impact of gender and age on *In vivo* virtual histology–intravascular ultrasound imaging plaque characterization (from the global virtual histology intravascular ultrasound [VH-IVUS] registry), Am. J. Cardiol. 103 (2009) 1210–1214, <https://doi.org/10.1016/j.amjcard.2009.01.031>.
- [73] M. Gudur, R. Kumon, Y. Zhou, C. Deng, High-frequency rapid B-mode Ultrasound imaging for real-time monitoring of lesion formation and gas body activity during high-intensity focused Ultrasound ablation, IEEE Trans. Ultrason. Ferroelectrics Freq. Control 59 (2012) 1687–1699, <https://doi.org/10.1109/TUFFC.2012.2374>.
- [74] R.E. Kumon, M.S.R. Gudur, Y. Zhou, C.X. Deng, High-frequency ultrasound M-mode imaging for identifying lesion and bubble activity during high-intensity focused ultrasound ablation, Ultrasound Med. Biol. 38 (2012) 626–641, <https://doi.org/10.1016/j.ultrasmedbio.2012.01.004>.
- [75] E.J. Peleppa, Ultrasonic tissue-type imaging of the prostate: implications for biopsy and treatment guidance, Colorado Bus. Mag. 4 (2008) 201–212, <https://doi.org/10.3233/CBM-2008-44-504>.
- [76] R.E. Kumon, M.J. Pollack, A.L. Faulk, K.O. Olowe, F.T. Farooq, V.K. Chen, Y. Zhou, R.C.K. Wong, G.A. Isenberg, M.V. Sivak, A. Chak, C.X. Deng, Vivo characterization of pancreatic and lymph node tissue by using EUS spectrum analysis: a validation study, Gastrointest. Endosc. 71 (2010) 53–63, <https://doi.org/10.1016/j.j.gie.2009.08.027>.
- [77] R.E. Kumon, K. Olowe, A.L. Faulk, F.T. Farooq, V.K. Chen, Y. Zhou, R.C.K. Wong, G.A. Isenberg, M.V. Sivak, A. Chak, C.X. Deng, EUS spectrum analysis for *In vivo* characterization of pancreatic and lymph node tissue: a pilot study, Gastrointest. Endosc. 66 (2007) 1096–1106, <https://doi.org/10.1016/j.j.gie.2007.05.052>.
- [78] M.C. Kolios, G.J. Czarnota, Potential use of ultrasound for the detection of cell changes in cancer treatment, Future Oncol. 5 (10) (2009) 1527–1532, <https://doi.org/10.2217/fon.09.157>.
- [79] A. Sadeghi-Naini, N. Papanicolaou, O. Falou, J. Zubovits, R. Dent, S. Verma, M. Trudeau, J.F. Boileau, J. Spayne, S. Iradj, E. Sofroni, J. Lee, S. Lemon-Wong, M. Yaffe, M.C. Kolios, G.J. Czarnota, Quantitative ultrasound evaluation of tumor cell death response in locally advanced breast cancer patients receiving chemotherapy, Clin. Cancer Res. 19 (8) (2013) 2163–2174, <https://doi.org/10.1158/1078-0432.CCR-12-2965>.
- [80] A. Sadeghi-Naini, L. Sannachi, H. Tadayyon, W.T. Tran, E. Slodkowska, M. Trudeau, S. Gandhi, K. Pritchard, M.C. Kolios, G.J. Czarnota, Chemotherapy-response monitoring of breast cancer patients using quantitative ultrasound-based intra-tumour heterogeneities, Sci. Rep. 7 (1) (2017), 10352, <https://doi.org/10.1038/s41598-017-09678-0>.
- [81] G.-Y. Li, Y. Cao, Mechanics of ultrasound elastography, Proc. R. Soc. A. 473 (2017), 20160841, <https://doi.org/10.1098/rspa.2016.0841>.
- [82] A.J. McCredie, E. Stride, N. Saffari, Ultrasound elastography to determine the layered mechanical properties of articular cartilage and the importance of such structural characteristics under load, in: Annual International Conference of the IEEE Engineering in Medicine and Biology Society, IEEE, Minneapolis, MN, 2009, pp. 4262–4265, <https://doi.org/10.1109/IEMBS.2009.5334589>, 2009.
- [83] C.-Y. Chung, J. Heebner, H. Baskaran, J.F. Welter, J.M. Mansour, Ultrasound elastography for estimation of regional strain of multilayered hydrogels and tissue-engineered cartilage, Ann. Biomed. Eng. 43 (2015) 2991–3003, <https://doi.org/10.1007/s10439-015-1356-x>.
- [84] X. Qian, T. Ma, M. Yu, X. Chen, K.K. Shung, Q. Zhou, Multi-functional ultrasonic micro-elastography imaging system, Sci. Rep. 7 (2017) 1230, <https://doi.org/10.1038/s41598-017-01210-8>.
- [85] S.S. Yengul, P.E. Barbone, B. Madore, Dispersion in tissue-mimicking gels measured with shear wave elastography and torsional vibration rheometry, Ultrasound Med. Biol. 45 (2019) 586–604, <https://doi.org/10.1016/j.ultrasmedbio.2018.07.002>.
- [86] H. Zhou, M. Goss, C. Hernandez, J.M. Mansour, A. Exner, Validation of ultrasound elastography imaging for nondestructive characterization of stiffer biomaterials, Ann. Biomed. Eng. 44 (2016) 1515–1523, <https://doi.org/10.1007/s10439-015-1448-7>.
- [87] F.W. Mauldin, M.A. Haider, E.G. Loba, R.H. Behler, L.E. Euliss, T.W. Pfeiler, C. M. Gallippi, Monitored steady-state excitation and recovery (MSSR) radiation force imaging using viscoelastic models, IEEE Trans. Ultrason. Ferroelectrics Freq. Control 55 (7) (2008) 1597–1610, <https://doi.org/10.1109/TUFFC.2008.836>.
- [88] Dalong Liu, E.S. Ebbini, Viscoelastic property measurement in thin tissue constructs using ultrasound, IEEE Trans. Ultrason. Ferroelectrics Freq. Control 55 (2) (2008) 368–383, <https://doi.org/10.1109/TUFFC.2008.655>.
- [89] E. Maksuti, E. Widmer, D. Larsson, M.W. Urban, M. Larsson, A. Bjällmark, Arterial stiffness estimation by shear wave elastography: validation in phantoms with mechanical testing, Ultrasound Med. Biol. 42 (2016) 308–321, <https://doi.org/10.1016/j.ultrasmedbio.2015.08.012>.
- [90] G.-Y. Li, Y. Zheng, Y.-X. Jiang, Z. Zhang, Y. Cao, Guided wave elastography of layered soft tissues, Acta Biomater. 84 (2019) 293–304, <https://doi.org/10.1016/j.actbio.2018.12.002>.
- [91] B.B. Guzina, K. Tuleubekov, D. Liu, E.S. Ebbini, Viscoelastic characterization of thin tissues using acoustic radiation force and model-based inversion, Phys. Med. Biol. 54 (13) (2009) 4089–4112, <https://doi.org/10.1088/0031-9155/54/13/009>.
- [92] M.W. Urban, I.Z. Nenadic, B. Qiang, M. Bernal, S. Chen, J.F. Greenleaf, Characterization of material properties of soft solid thin layers with acoustic radiation force and wave propagation, J. Acoust. Soc. Am. 138 (4) (2015) 2499–2507, <https://doi.org/10.1121/1.4932170>.
- [93] C.-C. Shih, X. Qian, T. Ma, Z. Han, C.-C. Huang, Q. Zhou, K.K. Shung, Quantitative assessment of thin-layer tissue viscoelastic properties using ultrasonic micro-elastography with lamb wave model, IEEE Trans. Med. Imag. 37 (8) (2018) 1887–1898, <https://doi.org/10.1109/TMI.2018.2820157>.
- [94] J. Prager, C.F. Adams, A.M. Delaney, G. Chanot, J.F. Tarlton, L.-F. Wong, D. M. Chari, N. Granger, Stiffness-matched biomaterial implants for cell delivery: clinical, intraoperative ultrasound elastography provides a ‘target’ stiffness for hydrogel synthesis in spinal cord injury, J. Tissue Eng. 11 (2020), 204173142093480, <https://doi.org/10.1177/2041731420934806>.
- [95] G.-C. Chun, H.-J. Chiang, K.-H. Lin, C.-M. Li, P.-J. Chen, T. Chen, Ultrasound elasticity imaging system with chirp-coded excitation for assessing biomechanical properties of elasticity phantom, Materials 8 (2015) 8392–8413, <https://doi.org/10.3390/ma8125458>.
- [96] K.P. Mercado, J. Langdon, M. Helguera, S.A. McAleavy, D.C. Hocking, D. Dalecki, Scholte wave generation during single tracking location shear wave elasticity imaging of engineered tissues, J. Acoust. Soc. Am. 138 (2015) EL138, <https://doi.org/10.1121/1.4927633>. –EL144.
- [97] A. Zareei, H. Jiang, S. Chittiboyina, J. Zhou, B.P. Marin, S.A. Lelièvre, R. Rahimi, A lab-on-chip ultrasonic platform for real-time and nondestructive assessment of extracellular matrix stiffness, Lab Chip 20 (2020) 778–788, <https://doi.org/10.1039/C9LC00926D>.
- [98] P.-L. Kuo, C.-C. Charng, P.-C. Wu, P.-C. Li, Shear-wave elasticity measurements of three-dimensional cell cultures for mechanobiology, J. Cell Sci. 130 (2017) 292–302, <https://doi.org/10.1242/jcs.186320>.
- [99] X. Hong, J.P. Stegemann, C.X. Deng, Microscale characterization of the viscoelastic properties of hydrogel biomaterials using dual-mode ultrasound elastography, Biomaterials 88 (2016) 12–24, <https://doi.org/10.1016/j.biomaterials.2016.02.019>.
- [100] X. Hong, R.T. Annamalai, T.S. Kemerer, C.X. Deng, J.P. Stegemann, Multimode ultrasound viscoelastography for three-dimensional interrogation of microscale mechanical properties in heterogeneous biomaterials, Biomaterials 178 (2018) 11–22, <https://doi.org/10.1016/j.biomaterials.2018.05.057>.
- [101] E.C. Hobson, W. Li, B.A. Julian, A.J. Putnam, J.P. Stegemann, C.X. Deng, Resonant acoustic rheometry for non-contact characterization of viscoelastic biomaterials, Biomaterials 269 (2021), 120676, <https://doi.org/10.1016/j.biomaterials.2021.120676>.
- [102] S.-L. Lu, P.-Y. Chao, W.-W. Liu, K. Han, J.C.-H. Cheng, P.-C. Li, Longitudinal shear wave elasticity measurements of millimeter-sized biomaterials using a single-element transducer platform, PLoS One 17 (4) (2022), e0266235, <https://doi.org/10.1371/journal.pone.0266235>.
- [103] G.-S. Jeng, C.-L. Yeh, C.-L. Lee, Y.-S. Yang, L.-Y. Tseng, P.-C. Li, Ultrasound shear-wave computed tomography for elasticity imaging, Appl. Phys. Lett. 121 (4) (2022), 043702, <https://doi.org/10.1063/5.0100628>.
- [104] D. Dutta, K.-W. Lee, R.A. Allen, Y. Wang, J.C. Brigham, K. Kim, Non-invasive assessment of elastic modulus of arterial constructs during cell culture using ultrasound elasticity imaging, Ultrasound Med. Biol. 39 (11) (2013) 2103–2115, <https://doi.org/10.1016/j.ultrasmedbio.2013.04.023>.
- [105] C.Y. Kuo, A. Eranki, J.K. Placome, K.R. Rhodes, H. Aranda-Espinoza, R. Fernandes, J.P. Fisher, P.C.W. Kim, Development of a 3D printed, bioengineered placenta model to evaluate the role of trophoblast migration in preeclampsia, ACS Biomater. Sci. Eng. 2 (2016) 1817–1826, <https://doi.org/10.1021/acsbiomaterials.6b00031>.
- [106] M. Tanter, D. Touboul, J.-L. Gennisson, J. Bercoff, M. Fink, High-resolution quantitative imaging of cornea elasticity using supersonic shear imaging, IEEE Trans. Med. Imag. 28 (2009) 1881–1893, <https://doi.org/10.1109/TMI.2009.2021471>.
- [107] H. Kanai, Propagation of spontaneously actuated pulsive vibration in human heart wall and *in vivo* viscoelasticity estimation, IEEE Trans. Ultrason. Ferroelectrics Freq. Control 52 (2005) 1931–1942, <https://doi.org/10.1109/TUFFC.2005.1561662>.

- [108] I. Nenadic, L. Mynderse, D. Husmann, M. Mehrmohammadi, M. Bayat, A. Singh, M. Denis, M. Urban, A. Alizad, M. Fatemi, Noninvasive evaluation of bladder wall mechanical properties as a function of filling volume: potential application in bladder compliance assessment, *PLoS One* 11 (2016), e0157818, <https://doi.org/10.1371/journal.pone.0157818>.
- [109] J. Brum, M. Bernal, J.L. Gennisson, M. Tanter, *In vivo* evaluation of the elastic anisotropy of the human Achilles tendon using shear wave dispersion analysis, *Phys. Med. Biol.* 59 (2014) 505–523, <https://doi.org/10.1088/0031-9155/59/3/505>.
- [110] M.J.S. Lowe, Matrix techniques for modeling ultrasonic waves in multilayered media, *IEEE Trans. Ultrason. Ferroelectrics Freq. Control* 42 (4) (1995) 525–542, <https://doi.org/10.1109/58.393096>.
- [111] J. Baranger, B. Arnal, F. Perren, O. Baud, M. Tanter, C. Demené, Adaptive spatiotemporal SVD clutter filtering for ultrafast Doppler imaging using similarity of spatial singular vectors, *IEEE Trans. Med. Imag.* 37 (7) (2018) 1574–1586, <https://doi.org/10.1109/TMI.2018.2789499>.
- [112] C. Demené, J. Robin, A. Dizeux, B. Heiles, M. Pernot, M. Tanter, F. Perren, Transcranial ultrafast ultrasound localization microscopy of brain vasculature in patients, *Nature Biomedical Engineering* 5 (3) (2021) 219–228, <https://doi.org/10.1038/s41551-021-00697-x>.
- [113] O. Villemain, M. Correia, D. Khraiche, I. Podetti, M. Meot, A. Legendre, M. Tanter, D. Bonnet, M. Pernot, Myocardial stiffness assessment using shear wave imaging in pediatric hypertrophic cardiomyopathy, *JACC (J. Am. Coll. Cardiol.): Cardiovascular Imaging* 11 (5) (2018) 779–781, <https://doi.org/10.1016/j.jcmg.2017.08.018>.
- [114] D. Cosgrove, F. Piscaglia, J. Bamber, J. Bojunga, J.-M. Correas, O. Gilja, A. Klauser, I. Sporea, F. Calliada, V. Cantisani, M. D'Onofrio, E. Drakonaki, M. Fink, M. Friedrich-Rust, J. Fromageau, R. Havre, C. Jenssen, R. Ohlinger, A. Säftou, C. Dietrich, EFSUMB guidelines and recommendations on the clinical use of ultrasound elastography. Part 2: clinical applications, *Ultraschall in der Medizin - European Journal of Ultrasound* 34 (3) (2013) 238–253, <https://doi.org/10.1005/s-0033-1335375>.
- [115] O. Villemain, J. Baranger, M.K. Friedberg, C. Papadacci, A. Dizeux, E. Messas, M. Tanter, M. Pernot, L. Mertens, Ultrafast ultrasound imaging in pediatric and adult cardiology, *JACC (J. Am. Coll. Cardiol.): Cardiovascular Imaging* 13 (8) (2020) 1771–1791, <https://doi.org/10.1016/j.jcmg.2019.09.019>.
- [116] M. Tanter, M. Fink, Ultrafast imaging in biomedical ultrasound, *IEEE Trans. Ultrason. Ferroelectrics Freq. Control* 61 (1) (2014) 102–119, <https://doi.org/10.1109/TUFFC.2014.2882>.
- [117] C. Papadacci, V. Finel, J. Provost, O. Villemain, P. Bruneval, J.-L. Gennisson, M. Tanter, M. Fink, M. Pernot, Imaging the dynamics of cardiac fiber orientation in vivo using 3D Ultrasound Backscatter Tensor Imaging, *Sci. Rep.* 7 (1) (2017) 830, <https://doi.org/10.1038/s41598-017-00946-7>.
- [118] J.C. del Alamo, D. Lemons, R. Serrano, A. Savchenko, F. Cerignoli, R. Bodmer, M. Mercola, High throughput physiological screening of iPSC-derived cardiomyocytes for drug development, *Biochim. Biophys. Acta Mol. Cell Res.* 1863 (7) (2016) 1717–1727, <https://doi.org/10.1016/j.bbamcr.2016.03.003>.
- [119] E.M. Strohm, N. Callaghan, N. Latifi, N. Rafatian, S. Funakoshi, I. Fernandes, M. Radisic, G. Keller, M.C. Kolios, C.A. Simmons, Non-invasive quantification of contractile dynamics in cardiac cells, spheroids and organs-on-a-chip using high frequency ultrasound, *bioRxiv* (2022), <https://doi.org/10.1101/2022.06.28.497094>, 2022.06.28.497094.
- [120] N. Ferri, P. Siegl, A. Corsini, J. Herrmann, A. Lerman, R. Benghozi, Drug attrition during pre-clinical and clinical development: understanding and managing drug-induced cardiotoxicity, *Pharmacol. Therapeut.* 138 (3) (2013) 470–484, <https://doi.org/10.1016/j.pharmthera.2013.03.005>.
- [121] M.L. Sutherland, K.M. Fabre, D.A. Tagle, The National Institutes of Health Microphysiological Systems Program focuses on a critical challenge in the drug discovery pipeline, *Stem Cell Res. Ther.* 4 (Suppl 1) (2013) I1, <https://doi.org/10.1186/scrt361>.
- [122] A. Akhtar, The flaws and human harms of animal experimentation, *Camb. Q. Healthc. Ethics.* 24 (4) (2015) 407–419, <https://doi.org/10.1017/S0963180115000079>.
- [123] B. Zhang, A. Korolj, B.F.L. Lai, M. Radisic, Advances in organ-on-a-chip engineering, *Nat. Rev. Mater.* 3 (8) (2018) 257–278, <https://doi.org/10.1038/s41578-018-0034-7>.
- [124] D.E. Ingber, Is it time for reviewer 3 to request human organ chip experiments instead of animal validation studies? *Adv. Sci.* 7 (22) (2020), 2002030 <https://doi.org/10.1002/advs.202002030>.
- [125] O. Mastikhina, B.-U. Moon, K. Williams, R. Hatkar, D. Gustafson, O. Mourad, X. Sun, M. Koo, A.Y.L. Lam, Y. Sun, J.E. Fish, E.W.K. Young, S.S. Nunes, Human cardiac fibrosis-on-a-chip model recapitulates disease hallmarks and can serve as a platform for drug testing, *Biomaterials* 233 (2020), 119741, <https://doi.org/10.1016/j.biomaterials.2019.119741>.
- [126] Y.R. Lewis-Israeli, A.H. Wasserman, M.A. Gabalski, B.D. Volmert, Y. Ming, K. A. Ball, W. Yang, J. Zou, G. Ni, N. Pajares, X. Chatzistavrou, W. Li, C. Zhou, A. Aguirre, Self-assembling human heart organoids for the modeling of cardiac development and congenital heart disease, *Nat. Commun.* 12 (1) (2021) 5142, <https://doi.org/10.1038/s41467-021-25329-5>.
- [127] S.M. Maffioletti, S. Sarcar, A.B.H. Henderson, I. Mannhardt, L. Pinton, L.A. Moyle, H. Steele-Stallard, O. Cappellari, K.E. Wells, G. Ferrari, J.S. Mitchell, G.E. Tyzack, V.N. Kotiadis, M. Khedr, M. Ragazzi, W. Wang, M.R. Duchen, R. Patani, P. S. Zammit, F.S. Tedesco, Three-dimensional human iPSC-derived artificial skeletal muscles model muscular dystrophies and enable multilineage tissue engineering, *Cell Rep.* 23 (3) (2018) 899–908, <https://doi.org/10.1016/j.celrep.2018.03.091>.
- [128] T. Kostrzewski, S. Snow, A.L. Battle, S. Peel, Z. Ahmad, J. Basak, M. Surakala, A. Bornot, J. Lindgren, M. Ryaboshapkina, M. Clausen, D. Lindén, C. Maass, L. M. Young, A. Corrigan, L. Ewart, D. Hughes, Modelling human liver fibrosis in the context of non-alcoholic steatohepatitis using a microphysiological system, *Communications Biology* 4 (1) (2021) 1080, <https://doi.org/10.1038/s42003-021-02616-x>.
- [129] J. Lee, S. Mehrrota, E. Zare-Eelanjeh, R.O. Rodrigues, A. Akbarnejad, D. Ge, L. Amato, K. Kiaeey, Y. Fang, A. Rosenkranz, W. Keung, B.B. Mandal, R.A. Li, T. Zhang, H. Lee, M.R. Dokmeci, Y.S. Zhang, A. Khademhosseini, S.R. Shin, Organ-on-a-Chip: a heart-breast cancer-on-a-chip platform for disease modeling and monitoring of cardiotoxicity induced by cancer chemotherapy (small 15/2021), *Small* 17 (15) (2021), 2170070, <https://doi.org/10.1002/smll.202170070>.
- [130] J.-H. Kim, G.H. An, J.-Y. Kim, R. Rasaei, W.J. Kim, X. Jin, D.-H. Woo, C. Han, S.-R. Yang, J.-H. Kim, S.-H. Hong, Human pluripotent stem cell-derived alveolar organoids for modeling pulmonary fibrosis and drug testing, *Cell Death Discovery* 7 (1) (2021) 48, <https://doi.org/10.1038/s41420-021-00439-7>.
- [131] C.F. Guimarães, L. Gasperini, A.P. Marques, R.L. Reis, The stiffness of living tissues and its implications for tissue engineering, *Nat. Rev. Mater.* 5 (5) (2020) 351–370, <https://doi.org/10.1038/s41578-019-0169-1>.